

# An Unsupervised Deep XAI Framework for Localization of Concurrent Replay Attacks in Nuclear Reactor Signals

Konstantinos Vasili\*, Zachery T. Dahm, Stylianos Chatzidakis

**Affiliation:** School of Nuclear Engineering, Purdue University, West Lafayette, IN 47907

**\*Corresponding author:** vasilik@purdue.edu

## Abstract

Next-generation advanced nuclear reactors are expected to be smaller in size and power output, relying extensively on fully digital instrumentation and control systems. These reactors will generate a large flow of information, conveying simultaneously various non-linear operational states. Ensuring data integrity against deception attacks is becoming more and more important for networked communication, cyber-physical control systems, and a requirement for safe operation. Current efforts to address replay attacks, a special kind of deception cyber event, almost universally focus on watermarking or anomaly detection approaches without further identifying the root cause of the anomaly. In addition, they rely mostly on synthetic data with uncorrelated Gaussian process and measurement noise and full state feedback, or are limited to univariate signals, signal stationarity, linear quadratic regulators, or other linear time-invariant state-space models, which may fail to capture unmodeled system dynamics. In the realm of regulated nuclear cyber-physical systems, additional work is needed on characterization and explainability of replay attacks using real data. Here, we propose an unsupervised explainable AI (XAI) framework based on a combination of an autoencoder and customized windowSHAP algorithm to fully characterize real-time replay attacks, i.e., detection, source identification, timing and type, of increasing complexity during a dynamic time-evolving reactor process. The proposed XAI framework was benchmarked on real-world datasets from Purdue's nuclear reactor, with up to six signals concurrently being replayed. In all cases, the XAI framework was able to detect and identify the number of signals being replayed and the duration of the falsification with 95% or better accuracy.

**Keywords:** replay attack, autoencoders, explainable AI, PUR-1, multivariate time series data

## Introduction

Currently, there is a growing trend in the nuclear industry toward advanced reactor designs, such as microreactors and small modular reactors. To make these designs cost competitive and operationally flexible, digital instrumentation and control, further supported by wired or wireless communication networks, will need to be implemented. These systems promise centralized or semi-autonomous control, real time monitoring, prognostics, diagnostics, and unattended operation [1][2][3][4]. Despite the numerous advantages of digital instrumentation and control, new challenges emerge, including the near impossibility of maintaining constant human surveillance over potential anomalies or cyber events within the digital system [5]. Unlike conventional information technology (IT) systems, where the main focus is the protection of network data, cyber events on critical, networked control infrastructure could affect not only the data but also physical and control processes through a variety of different ways, potentially causing economic loss, (e.g., due to unnecessary shutdown of the reactor) or equipment damage [6] [7]. The nuclear industry has been a target for cyber threats for many years [8][9]. It is worth noting the infamous Stuxnet malware detected in 2010, which affected the digitized industrial control system of a nuclear facility [10] [11] along with other non-nuclear facilities around the world. Other examples include the Korea Hydro and Nuclear Power incident in 2014 [12], the Davis-Besse NPP event in 2011 [13], and the Browns Ferry NPP Unit 3 incident in 2006 [14]. These cyber incidents suggest that the introduction of new vulnerabilities to nuclear systems, previously non-existent due to analog-base operation, is an increasing concern [15].

Teixeira et al. [6] present an overview of cyber events that could compromise control systems and define a 3-dimensional cyber physical attack space comprising knowledge, disclosure, and disruption resources. The main properties of an attack include violation of data confidentiality, integrity, and availability. Characteristic example of data availability violation is a Denial of Service (DoS) attack [16] [17] where an adversary prevents data from reaching their destination. Examples of data integrity violations include deception attacks such as False Data Injection (FDI) [18] [19] and replay attacks [20] [21]. FDI attacks have received attention recently and a review of state-of-the art against modern power systems can be found in [22]. A replay attack, a subset of deception threats, requires the adversary to deploy disclosure and disruption resources but not prior system knowledge, making it particularly concerning and difficult to detect due to its simplicity and effectiveness. During a replay attack, the adversary intercepts an unknown amount of information and resends it at a later time to deceive the operators for the current system state [6], [21]. Unlike an FDI attack, which injects conceptually erroneous data into the system, a replay attack resends valid data from a past operational mode, making it harder to detect and flag as an anomaly. During Stuxnet, though not primarily a replay attack, recorded normal data were replayed to the monitoring system to create the illusion that the system was operating normally, while an even more sophisticated attack was ongoing.

Over the past years, several techniques have been proposed to identify anomalies caused by replay attacks, including watermarking [20] [21] [23] [24] and data-driven approaches [25] [26] [27] [28]. In one of the earliest works in the field, Mo and Sinopoli, 2009 [20] investigated a discrete, linear time invariant, Gaussian control system for anomaly detection. They proved that the difference between the actual and predicted measurements from a Kalman filter follows a Gaussian distribution. Subsequently, a  $\chi^2$  failure detector was used for intrusion detection by adding random noise to the signal and comparing the difference to a threshold within a predefined window length. Yao and Smidts, 2020 [21] extended this approach by adding a second  $\chi^2$  detector to include classification of the anomaly into FDI or other types. While successful, both studies relied on linearized mathematical models, uncorrelated Gaussian noise, and required specific parameterizations to represent the system non-linear dynamics. Additionally, signal stationarity was assumed, and synthetic data were used for proof of concept.

Data driven techniques have also been proposed for detection of anomalies caused by replay attacks across various domains, including smart cities and industrial control systems. AA Elsaedy et al. (2020) developed a Deep Learning (DL) pipeline for detecting anomalies in smart cities [25]. A multi-sensor infrastructure was designed to collect multivariate data, and various DL architectures, including Convolutional Neural Networks (CNNs), were trained as a binary classification problem to classify the time series as normal or attack. Of relevance to our work, Gargoum et al. [26] propose a data driven, two stage framework for anomaly detection and verification. The approach combines matrix profile-based change-point detection with a convLSTM architecture to distinguish normal from replayed sensor measurements. The framework introduces spatio-temporal features to subsequences of the time series flagged as replay attacks to verify the detection. Despite its novelty, the method appears to be applied to a single feature and does not address scenarios involving multi-sensory or multivariate environments, where replay attacks may target arbitrary combinations of signals. Furthermore, even if separate frameworks were deployed to monitor each signal, the approach would fail in scenarios where anomalies are contextual, flagged by the absence of expected inter-signal correlations rather than deviations in individual signal patterns.

Wang et al. [27] explored an Long Short-Term Memory (LSTM) framework for predicting and detecting FDI and replay attacks in multivariate times series (MTS) data of an industrial control process. The framework successfully identified replayed sequences by comparing predictions with a predefined error threshold. However, it considered a scenario where all the signals were falsified creating clearly distinguishable patterns, while unable to identify specific signals or the timing and duration of the attack. To address this, Dahm et al., 2025 [28] extended the approach by adding interpretability to an LSTM predictive framework for replay attack scenarios in MTS data from the PUR-1 nuclear reactor. The framework, successfully demonstrated using real data from PUR-1, identified nonstationary, concurrent replay attack scenarios of increasing complexity by extracting Shapley values to interpret the difference

between a critical signal prediction and the actual signal value. Despite its success, the framework relies on the prediction of a single critical signal not known a priori to the adversary, which limits its applicability in scenarios where the critical signal is itself the target of a possible attack. Other approaches propose clustering based statistical methods [29] [30] and classical ML techniques such as SVM [31]. Although suitable for their specific applications, these methods do not consider the time component and therefore are not suitable for real time monitoring.

Replay attacks, as a specific subclass of cyber threats, fall into the general field of anomaly detection, and tools from this field are typically employed to address them. With advancements in computational units observed in recent years, significant attention has been dedicated to anomaly detection using AI/ML. A comprehensive review is listed in this survey [32]. Among various approaches, unsupervised methods using Autoencoders (AE) have shown strong performance, especially in cases where abnormal events are rare. A promising research direction explores the combination of AE with SHAP (Shapley Additive exPlanations) analysis to provide interpretable insights into the deviations from normal patterns [33] [34] [35]. However, despite its significance, the absence of the time dimension in SHAP analysis, combined with deeper architectures, has not received adequate attention, especially for time-evolving critical processes. In this work, we aim to fill this gap by combining and expanding two individually proven techniques into a unified, robust, and efficient framework. We employ a deep unsupervised encoder-decoder architecture which, combined with a modified explainable AI (XAI) module, enables real-time reconstruction error analysis and characterization of signal-level replay attack scenarios of increased complexity during a dynamic, time-evolving reactor operation. The framework extends beyond a binary classification task, by quantifying feature importance across time and feature space. It identifies a general condition that triggers deviation from expected reactor behavior and further investigates each signal's contribution by utilizing a dynamically updated baseline condition to calculate Shapley values in time and feature space. The proposed approach was benchmarked against real-world data from Purdue's nuclear reactor (PUR-1) and can be extended to any control system with predictable operational modes.

The remainder of the paper is organized as follows. Section II presents the use case, the PUR-1 system, the data extraction and the simulation of the attack scenarios. Section III introduces the methodology employed to detect the replayed sequences in each scenario. Section IV describes the implementation of each module in the methodology. Section V details the results of the proposed framework along with the discussion, and lastly Section VI concludes the paper.

## **Use case**

### **Scenario**

The use case involves injecting multiple replay attacks into different sensors using data recorded from a past steady state condition. This experimentally simulates an adversary

attempting to deceive an operator into believing that the system remains at high power during a shutdown process. The event starts when the SCRAM button is activated. This cuts the magnet current to the control rods, which are then rapidly inserted into the reactor core. The control rods are made of neutron absorbing material and immediately terminate the reactor's heat production process. From that point, the reactor power is due to residual heat generated from precursor concentrations. In a normal process, the visualized sensor readings depict a rapidly changing condition, as shown in Figure 1 (left). The conceptual cyber scenario is shown in Figure 1 (right), where the green line indicates the SCRAM button activation, the red line represents the expected response, and the blue line shows the observed behavior resulting from the cyber event.

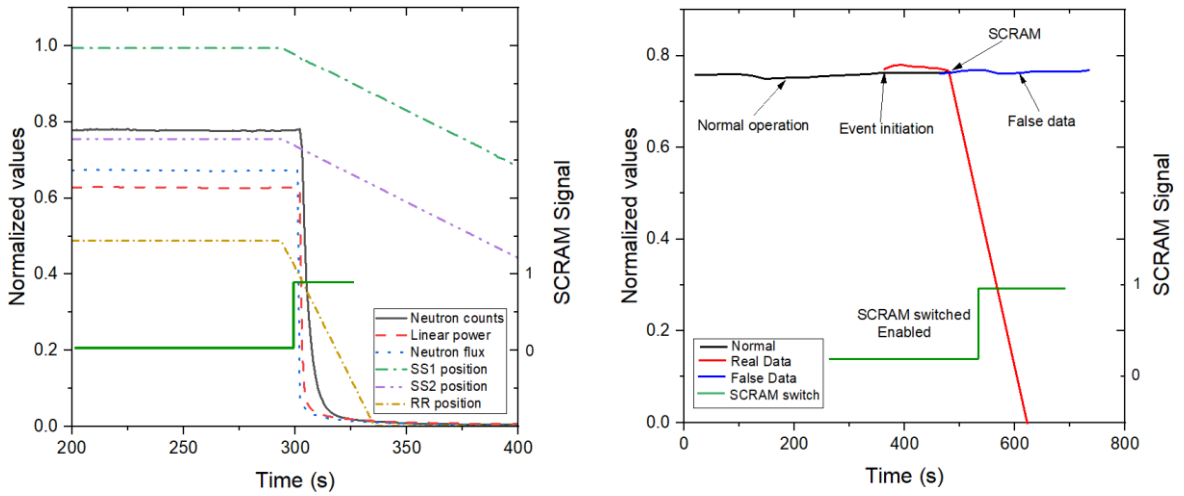


Figure 1: Variation in neutron counts after a forced shutdown (SCRAM) (left). Cyber event initiation represented by the blue line where the shutdown process is not followed by decreasing values (right).

To explore the efficiency of the proposed framework for this scenario, replay attack events of increasing complexity were experimentally simulated. A set of  $n$  sensor measurements from a control system can be represented as time series data in the following form:

$$X(t) = [x_1(t), x_2(t), \dots, x_n(t)]$$

Where each element  $x_i(t)$  represents the reading from the  $i$ -th sensor at time  $t$ . Under the assumption that the attacker has access to the system, the replay attack is carried out in two stages, as described in relevant literature [26], [36]. In the first stage, the system is intercepted, and  $k$  unknown signals are recorded over an unknown time interval  $I$ . The recorded set can be represented as:

$$\tilde{X}(t) = [\tilde{x}_1(t), \tilde{x}_2(t), \dots, \tilde{x}_k(t)], \quad t \in I$$

The time interval  $I$  is defined as:  $I = [t_{start}, t_{start} + T]$ ,

Where  $t_{start}$  is the start time of the recording, and  $T$  is the period of the recorded signal.

In the second stage, the attacker injects the recorded set  $\tilde{X}$  at a later time interval denoted as:  $I_{attack} = [t_{attack}, t_{attack} + NT]$ , where  $t_{attack}$  denotes the attack start time and  $N$  represents the number of times the recorded set is repeated. If  $N = 1$ , the attack can be regarded as a delay attack. For our use case  $k$  starts with one and increases to six signals: neutron counts (ch.1), reactor power (ch. 3), neutron flux (ch. 4), the regulatory rod (rr-position), the SS1 rod, and the SS2 rod. It is assumed that these signals will be primarily a target for a cyber-attack, as they are typically monitored by operators on the control console. The recorded time interval  $I$  is selected during a steady state condition prior to the SCRAM event. The period  $T$  is set to 20 seconds of steady state operation,  $t_{attack}$  is set just after the SCRAM button is pressed, approximately around 300 s, and  $N$  is set to 5, resulting in 100 seconds of replayed signals covering the entire SCRAM event (Figure 2). The selection of the above parameters (timing, period and number of signals) can lead to varying effects, creating different attack scenarios which may mislead the operator about the true reactor condition. Depending on the operator's response, the potential damage may include huge economic losses or even human loss, therefore the significance of correctly and promptly identifying the replay attack is evident. After the attack, all signals return to normal values, which are low sensor readings due to the large negative reactivity inserted by the control rods.

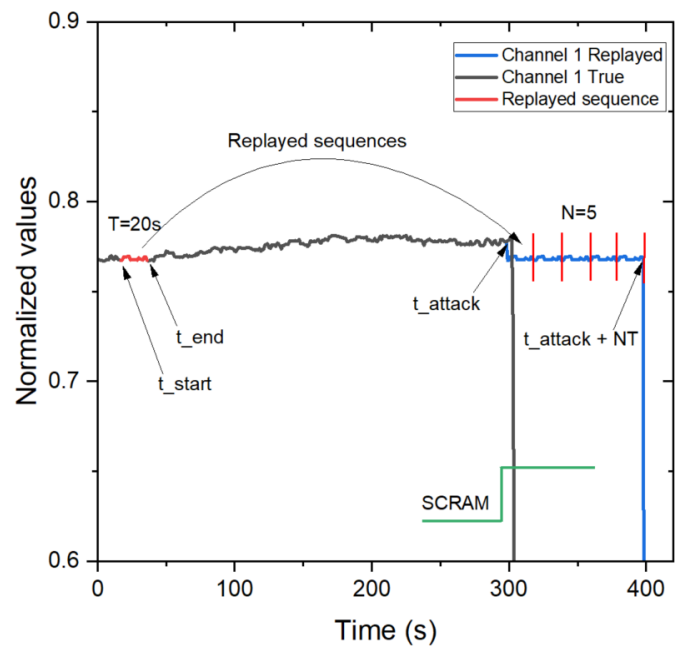


Figure 2: Example of a replay attack scenario for Channel 1. Applying the same process to additional signals simulates concurrent replay attacks of increasing complexity.

After a SCRAM process is initiated, although the control rods are inserted into the reactor core in the course of a few seconds, Figure 1 shows that the rr rod appears to insert immediately, while the SS1 and SS2 rods are shown to last around 300 seconds until fully inserted. This delay is primarily due to the control rod drivers rather than the

rod movements themselves, creating a unique pattern that helps the reactor operator to identify a SCRAM process on the console.

## PUR-1

Real reactor datasets cannot be easily found in the literature, and most of the work reported in the nuclear domain relies on simulated or synthetic data with limited physical or artificial inconsistencies, e.g., noise, null values and outliers, resulting in near perfect datasets for data-driven testing [37] [38] [39] [40] [41]. Here, we leverage Purdue’s University research reactor PUR-1 (Figure 3) [42] [43]. PUR-1 is a pool-type reactor licensed to operate up to 10 kWth continuous power and is the only reactor in the United States with a fully digital instrumentation and control system, which allows for real-time data access and remote monitoring. A digital twin [44] is enabling data collection of more than 2000 parameters per sampling frequency, in real time via a monitoring workstation (Figure 3).

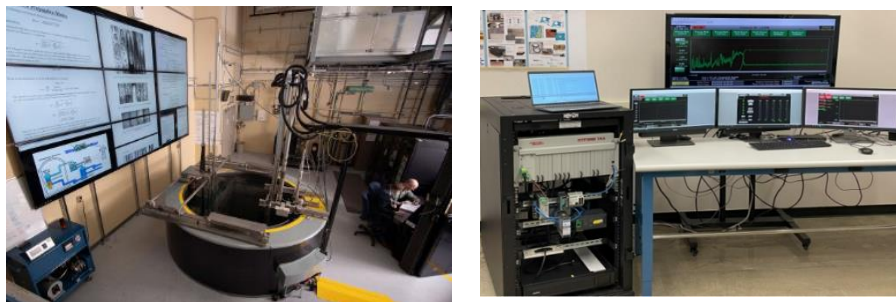


Figure 3: PUR-1 facility (left). Digital twin away from reactor building with no direct line of sight (right).

PUR-1 is only one component of a cyber-physical system consisting of five layers, which includes various other elements like equipment, controllers, network connections and communication protocols (Figure 4) [43]. Layers 0 to 3 are located inside the PUR-1 facility, while Layer 4 is located in a separate building with no direct line of sight to the reactor facility. The reactor operation dynamics can be regarded as a multidimensional temporal sequence of sensor readings generated from Layers 0 to 3. Data collection, analysis, ML training and testing occur at layer 4. A fundamental requirement for any cyber event, including FDI and replay attacks, is the intruder’s ability to have gained access to the network. For our use case, we assume the intruder has *a priori* system access at Layer 1 (but not at Layer 0) and can consequently record signals of interest through an entry point, and replay them at a later time.

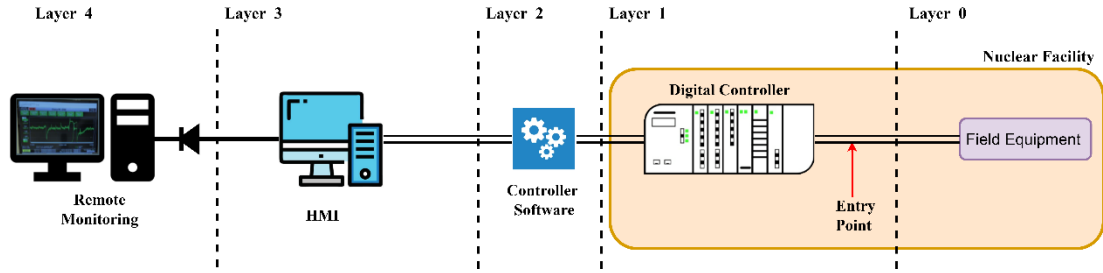


Figure 4: Cyber physical system architecture for PUR-1 cybersecurity testing.

Figure 5 presents the architecture that was developed to inject replay attacks and collect falsified data [43]. The architecture consists of two sections: (i) the Remote Location (left), where an attacker’s PC connects to the monitoring workstation via a network switch to enable the injection of false data; and (ii) the Control Room (right), which hosts the real-time reactor data network, including controllers, sensors, human-machine interfaces (HMIs), operational processes, and incoming signals used for decision-making [28][43].

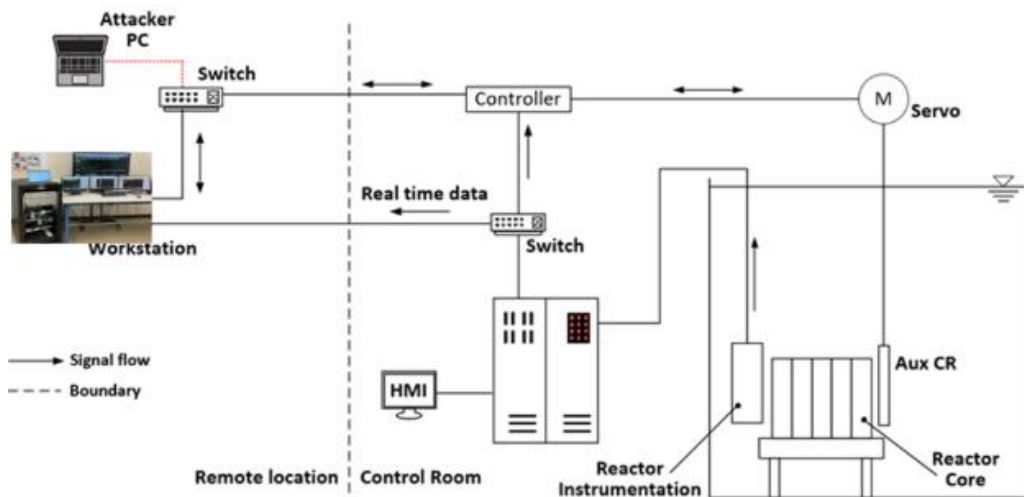


Figure 5: Architecture for injecting false data.

## Data

The data are extracted from the digital twin workstation (Figure 3) in tabular format capturing either the full set or a subset of available signals. Each row corresponds to a sampling frequency of one second, with columns representing different signals, collectively forming a MTS dataset that reflects the reactor operational condition at each time step. The high dimensionality of the dataset, which exceeds 2,000 signals, leads to increased computational costs and potential performance concerns, therefore, reducing the number of signals used for model training is necessary. We identified and

selected nine key signals that most accurately represent the reactor's functionality. The selected signals are shown in Table 1.

The operational data collected are subject to various artifacts such as fluctuations, outliers, null values, and noise. These inconsistencies arise from multiple sources, such as limitations or imperfections in the data collection instruments, and the inherent complexity of the monitoring system. Additionally, variability in human operation and decision-making contributes to data heterogeneity, as different operators may respond differently under similar conditions, a behavior reflected in the recorded data. The frequency and nature of these artifacts can also vary with the reactor's operational mode, whether in shutdown or any other active operation.

Table 1: Signals used for the training, testing and falsification

Feature	Units	Description
Neutron counts	1/s	Neutron counts per second as measured by channel 1
Linear power	%	Reactor power as measured by channel 3
Neutron flux	%	Neutron flux as measured by channel 4
ss1-position	cm	Distance an electromagnet has removed SS1 from the core
ss2-position	cm	Distance an electromagnet has removed SS2 from the core
rr-position	cm	Distance an electromagnet has removed RR from the core
rr-active-state	-	Categorical with three discrete values (insert-withdraw-steady)
ss1-active-state	-	Categorical with three discrete values (insert-withdraw-steady)
ss2-active-state	-	Categorical with three discrete values (insert-withdraw-steady)

A total of 47 full power cycle datasets were collected and used for the initial training of the algorithms. Each dataset contains approximately 5700 seconds (1.5 hours) of reactor operation, spanning start up to shutdown and including transient and steady state conditions at various power levels (Figure 6). Additionally, a collection of 24 SCRAM datasets, each approximately 800 seconds, was obtained to capture SCRAM occurrences at various power levels (Figure 7).

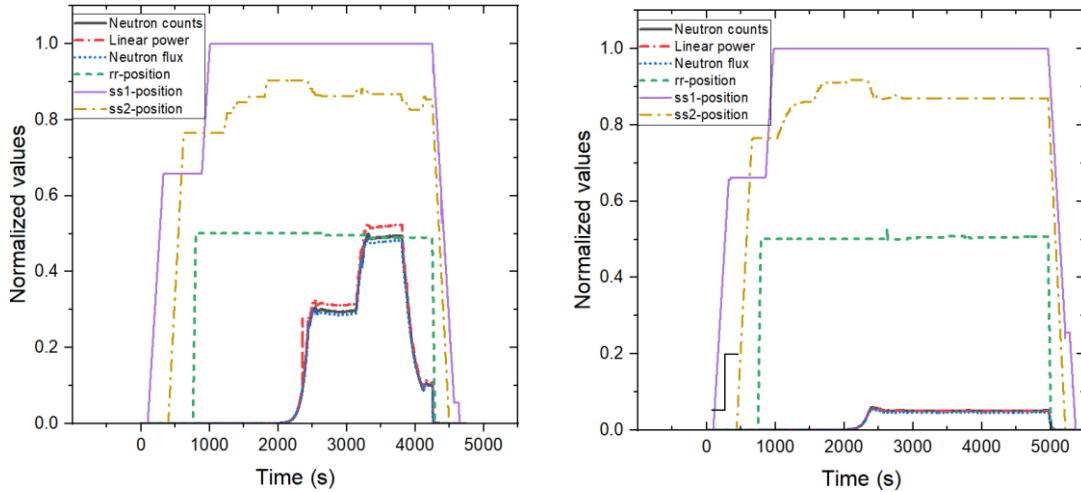


Figure 6: Examples of signal value variations across different full power cycles of PUR-1 operation.

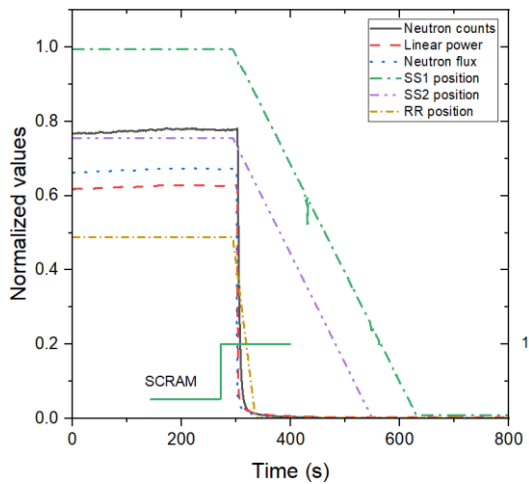


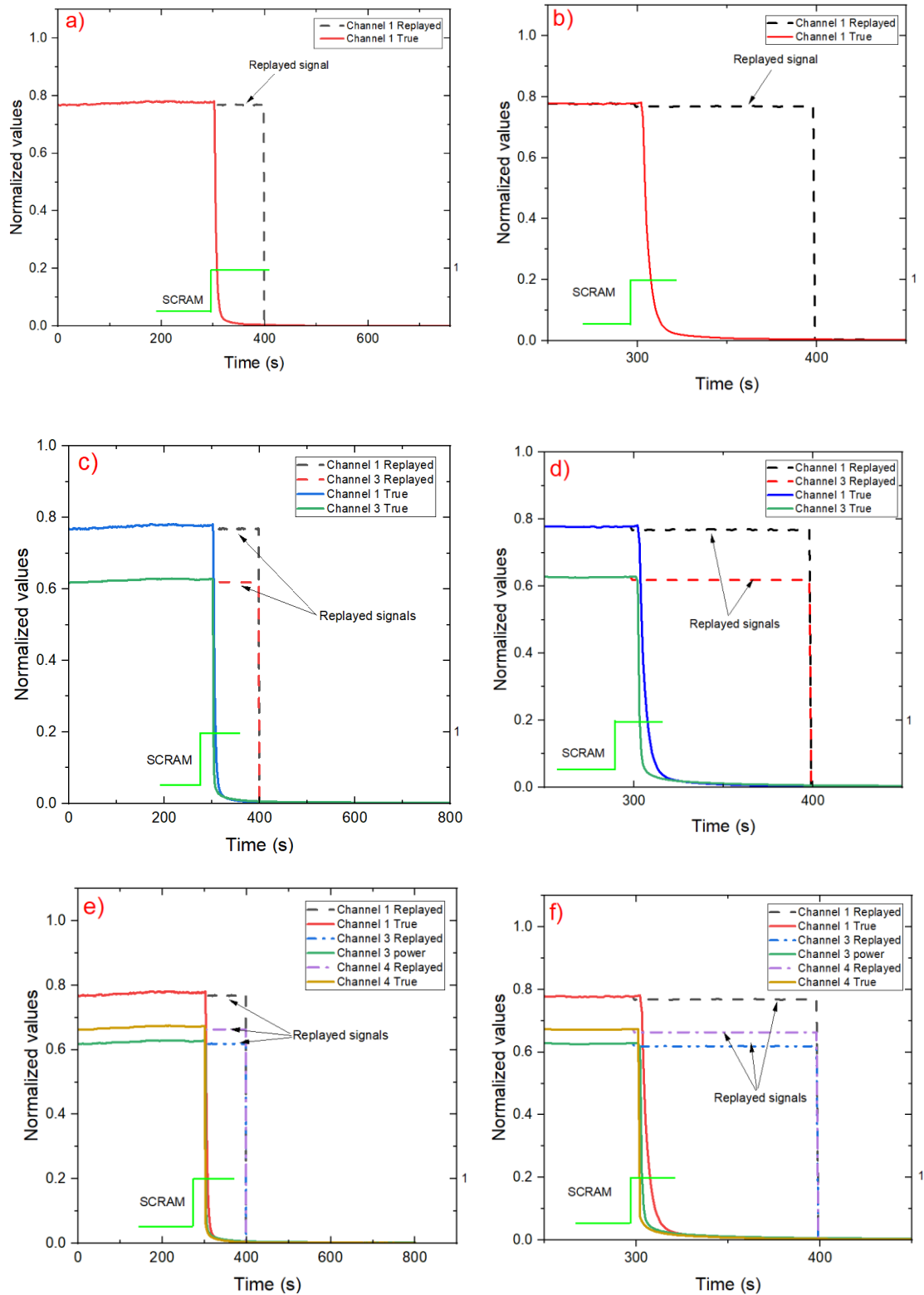
Figure 7: Expected signal behavior during a SCRAM event.

Following the process described in the scenario section, six replayed datasets were generated each involving an increasing number of falsified signals:

1. Replay#1: Replay attack of one signal (ch.1)
2. Replay#2: Replay attack of two signals (ch.1, ch.3)
3. Replay#3: Replay attack of three signals (ch.1, ch.3, ch.4)
4. Replay#4: Replay attack of four signals (ch.1, ch.3, ch.4, rr)
5. Replay#5: Replay attack of five signals (ch.1, ch.3, ch.4, rr, SS1)
6. Replay#6: Replay attack of six signals (ch.1, ch.3, ch.4, rr, SS1, SS2)

Out of the nine signals listed in Table 1, the three control rod active states remained unchanged across all cases to allow the algorithm to detect deviations from the normal case. Figure 8 presents the six simulated datasets. All signal values have been normalized to account for signal variability and ensure consistent visualization. Each dataset is divided into two panels: The left side displays the full 800 seconds of the SCRAM operation under the replay attack. The right side presents the same condition

restricted to the critical time frame in which the SCRAM is happening (300-400 seconds).



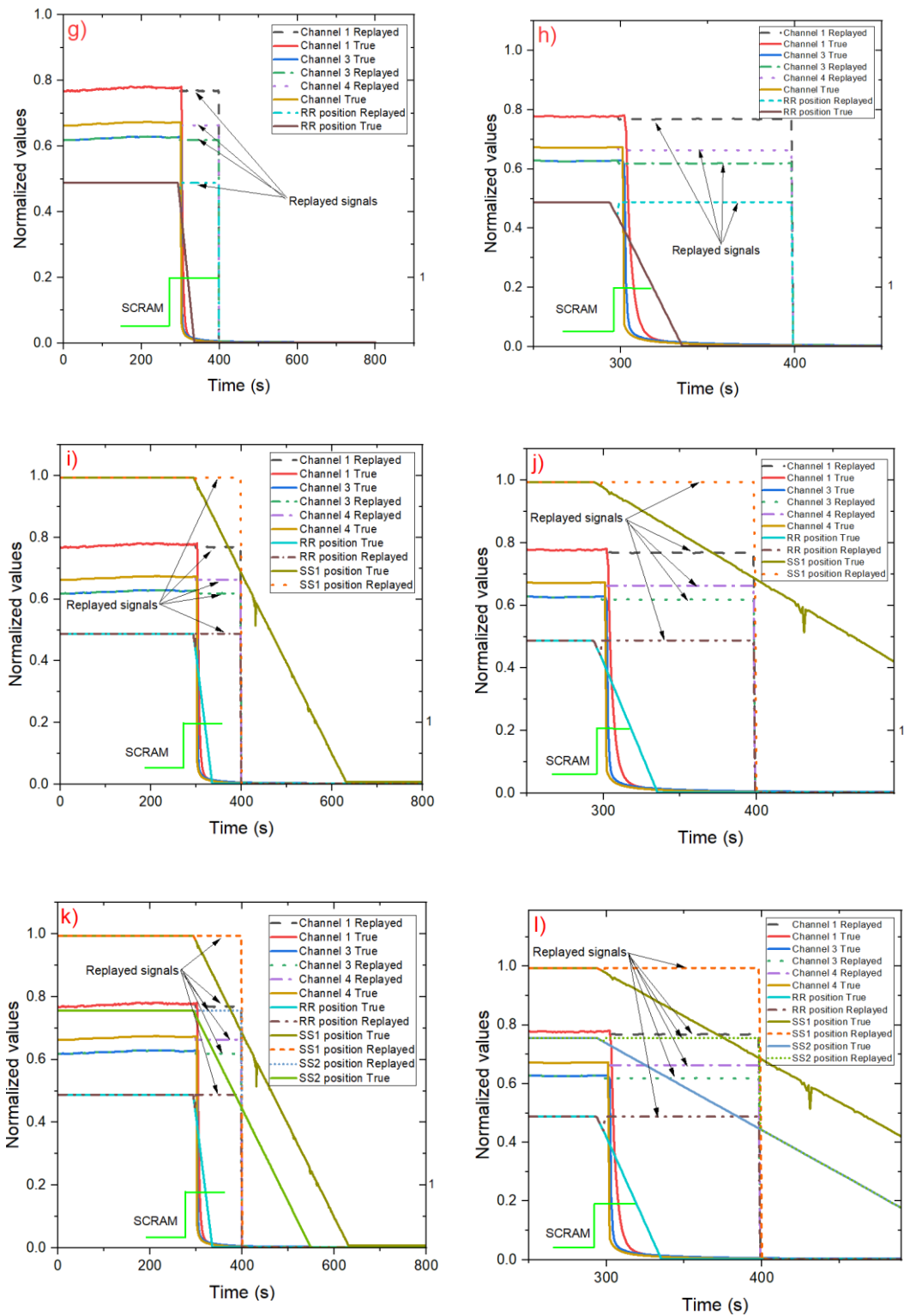


Figure 8: Replay attack one signal (a-b); Replay attack two signals (c-d); Replay attack three signals (e-f); Replay attack four signals (g-h). Replay attack five signals (i-j). Replay attack six signals (k-l). All signal values have been normalized to account for differing value ranges and facilitate visualization.

## Methodology

The proposed framework consists of three modules. The first module leverages a deep AE architecture composed of layers with time sequence learning capabilities, to form a reconstructive model of PUR-1 from the nine signals in Table 1. The second module analyzes the reconstructive model by comparing it with live data and decides whether a deviation from normal expectation is in place. The third module provides local interpretability for attack type, source identification, duration and timing information, and is based on a customized SHAP analysis for MTS data. The entire framework is presented in Figure 9.

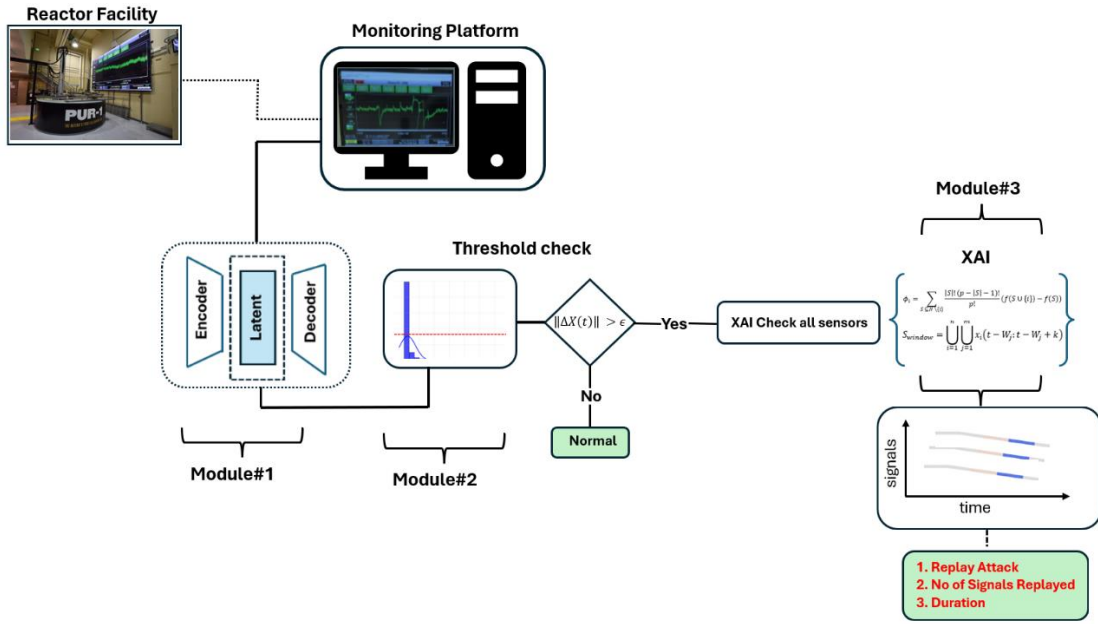


Figure 9: Methodology workflow

### Module 1: Reconstructive Modeling of Reactor Behavior

The first module involves training a deep AE architecture exclusively on normal data to allow the system to learn expected reactor behavior. By using a large number of full reactor power cycles (Figure 6), a model is constructed capturing the inherent dynamics, correlations, and interdependencies of sensor signals at all possible reactor conditions (startups, steady states, transients, shutdowns). The trained model learns to reconstruct signal values based on input signals. Let

$$X(t) = [x_1(t), x_2(t), \dots, x_n(t)] \quad t \in I$$

represent the set of  $n$  sensor measurements over the interval  $I$ , where  $x_i(t)$  denotes the reading from the  $i$ -th sensor. A reconstructive model  $f$  is trained under normal operational conditions on historical data to learn the functional mapping:

$$\hat{X}(t) = f(X(t))$$

Where  $\hat{X}(t)$  is the model’s reconstruction for the set  $X(t)$  over the same time interval  $I$ . The model is optimized by adjusting its weights and biases to minimize the error between the original and the reconstructed data for the fixed time interval  $I$ , over the entire length of the training data, such that:

$$\min_f \mathbb{E}[\|X(I) - \hat{X}(I)\|]$$

Where  $\|\cdot\|$  represents a norm appropriate to quantify similarities between two given vectors like mean squared error or absolute error. To optimize the reconstruction accuracy and ensure adaptability, we explored an appropriate AE architecture capable of capturing temporal dependencies in a multisensory dynamic environment. The fundamental concept of an AE is to generate a lower dimensional representation of the input time series through a sequence of neural layers, and then reconstruct it back to its original dimensional space.

A number of methods have demonstrated effectiveness in capturing temporal dependencies in MTS data, with characteristic examples being the Autoregressive Moving Average models and their variants, correlation-based, and ensemble methods [45][46][47][48][49]. Despite their success, AE architectures have gained attention and have become the standard approach for unsupervised anomaly detection via reconstruction in time series data, due to their ability to generalize and robustness to noise [50] [51]. Although not originally designed for anomaly detection, AE were introduced in the work of Rumelhart et al., 1986 [52] as a novel method for dimensionality reduction and representation learning, with applications on image storage and transmission. Their application for anomaly detection became prominent post 2010 with advancements in efficient deep learning architectures and computational units. In one of the first studies, Sakurada et al., 2014 [53] show that AE can effectively detect anomalies through nonlinear dimensionality reduction. The process involves training a mirrored network of neural layers with normal data, which enables the network to learn standard behavior of the system. At inference, sequences are reconstructed and deviations from the trained behavior are flagged as potential anomalies. In [50][54] unsupervised frameworks based on AE for anomaly detection and diagnosis in MTS are proposed with improved results when compared to baseline methods. Despite their performance, these methods do not consider patterns when abnormalities are flagged, or are assuming simplified assumptions regarding the root cause of the abnormal event. Therefore, they are not applicable to scenarios where interpretability is required at full scale.

AEs consist of an encoder, which compresses the input data by performing dimensionality reduction; a latent representation, which captures the most important patterns in the lower dimensional data; and a decoder, which reconstructs the data from the latent space back to their initial dimensions. Due to the wide range of applications, a number of different AE architectures have been proposed, each for a specific purpose. Most significant examples include vanilla AE, deep AE, convolutional AE, RNN-based AE, LSTM AE and Variational AE. A full taxonomy of architectures and uses can be found in this work [55]. In our study, LSTM layers [56] are employed within the AE

architecture to capture the temporal dependencies and accurately reconstruct the sequences. LSTM networks are a specific type of Recurrent Neural Network (RNN) [57], designed to overcome the vanishing gradient problem, which is commonly encountered in traditional RNNs, where the small gradients compromise the training process [58] [59]. LSTM networks introduce a memory and a hidden state, along with input, output, and forget gates that selectively discard or retain information from the memory cell. This architecture makes LSTMs well-suited for time series data, and ideal for modeling control systems with time-dependent patterns, such as reactor conditions, due to their ability to capture long and short term temporal dependencies. The equations governing the LSTM cell at a timestep  $t$  are:

$$\begin{aligned}
f_t &= \sigma(W_f x_t + U_f h_{(t-1)} + b_f) \\
i_t &= \sigma(W_i x_t + U_i h_{(t-1)} + b_i) \\
\tilde{c}_t &= \tanh(W_c x_t + U_c h_{(t-1)} + b_c) \\
c_t &= f_t \odot c_{(t-1)} + i_t \odot \tilde{c}_t \\
o_t &= \sigma(W_o x_t + U_o h_{(t-1)} + b_o) \\
h_t &= o_t \odot \tanh(c_t)
\end{aligned}$$

Where  $f_t$  is the forget gate,  $i_t$  is the input gate,  $\tilde{c}_t$  is the candidate cell,  $c_t$  is the update cell,  $o_t$  is the output cell,  $h_t$  is the hidden state,  $\sigma$  is the activation function,  $W_f, W_i, W_c, W_o, U_f, U_i, U_c, U_o$  are the weights matrices and  $b_f, b_i, b_c, b_o$  are the bias terms.

## Module 2: Reconstruction Error Analysis

The second module involves analyzing the errors of the reconstructive model from module 1 as a quantitative measurement for potential anomalies in the system. An advantage of using an AE architecture in the first module is that AEs are trained exclusively on normal operational data, eliminating the need to obtain rare or hard to find anomalies. Furthermore, AEs enable the detection of previously unseen anomalies without prior knowledge of what the data represents, removing the need to manually label known irregularities in the system. Reconstruction error analysis has been successfully demonstrated in relevant studies. This study [60] presents an efficient AE methodology to predict potential anomalies in the cooling system of a simulated PWR, based on the reconstruction error between unseen data and trained data. Similar studies in the nuclear domain include [61] [62] [63], where the large reconstruction error indicates a potential anomaly for their specific cases.

The main difference in our study is that the anomaly does not represent an obvious trend as time advances, but rather the lack of signal intercorrelation at a specific dynamic condition, which is ultimately driven by reactor operation. In this context, the replay attack has a conceptual effect [32], which only a trained operator with knowledge over the system can recognize. This distinction is important because it highlights the fact that anomalies would remain undetected by methods that rely solely on temporal patterns. The replay attack becomes effective once the data deviate significantly from the true condition, affecting the decision-making process, which potentially may lead

to unsafe reactor operation. To identify the replay attack first a metric which will trigger a flag at a given time is required. Let's assume a modified measurement vector:

$$\tilde{X}(t) = [\tilde{x}_1(t), \tilde{x}_2(t), \dots, \tilde{x}_n(t)]$$

where  $\tilde{x}_i(t)$  represents the replayed value of the  $i$ -th sensor at time  $t$ . The deviation introduced by the replay attack is given by:

$$\Delta X(t) = \tilde{X}(t) - X(t)$$

Where  $\tilde{X}(t)$  is the reconstructed data of  $X(t)$  at time  $t$ . An anomaly is flagged for a potential replay attack if:

$$\|\Delta X(t)\| > \epsilon, \quad \text{for some } I$$

Where  $I$  is a fixed time interval within the time series, and  $\epsilon$  is the minimum deviation required to cause the system's response. The threshold  $\epsilon$ , defines the sensitivity of the system and was evaluated as part of the hyperparameter tuning in the training data. Module 2 continuously evaluates the residual errors at a predefined window over the entire time series. Sections of the time series that fall below the threshold are considered normal reactor operation. For sequences that fall above the error, a post hoc interpretability analysis is employed to define whether patterns are in place that justify a replay attack in the system.

### **Module 3: Source and Timing Identification with Post Hoc Explainability**

In module 2 the system identifies a condition that deviates from the normal patterns based on the reconstruction error at a  $t$ -window sequence at time  $t$ . Detecting a deviation alone does not confirm a replay attack and certainly does not identify the source, as deviations can arise from a number of other factors such as operational changes, noise in the system or sensor malfunction. In this module, we introduce a modified SHAP analysis optimized for MTS data to add a layer of explainability and investigate the source of falsified sensors and the duration of the attack.

While AE and other AI/ML algorithms have been successfully used in data driven applications in a variety of different engineering and industrial problems [32], their lack of explainability, especially in considering multi signal monitoring and human-scale explanation, complicates their adaption in critical infrastructure [64]. Moreover, research conducted in [65] [66] has shown that lack of trust in advanced data analytics techniques can be attributed to the difficulty of gaining clear insights from such models. To fill this gap, SHAP analysis has emerged recently from game theory as a model agnostic framework designed to explain ML predictions [67] [68]. The framework quantifies feature contributions to the prediction of any ML model by assigning Shapley values to each feature, which either offset or support the prediction. SHAP was initially introduced to provide global explanations. As the models were becoming more complex the focus shifted towards instance-specific explanations [33]. In our study, we emphasize the need for time sequence level explanations in cases where the underlying system dynamics change over time.

The Shapley value for a given feature  $i$  is:

$$\phi_i = \sum_{S \subseteq N \setminus \{i\}} \frac{|S|! (p - |S| - 1)!}{p!} (f(S \cup \{i\}) - f(S))$$

Where,  $\phi_i$  represents the Shapley value calculated for feature  $i$ ,  $p$  is the total numbers of features in the dataset,  $S$  is all possible subsets (or coalitions) of features that don't include  $i$ ,  $|S|$  represents the number of features in subset  $S$ , and  $f(S \cup \{i\}) - f(S)$  is the marginal contribution of feature  $i$  to subset  $S$ . The summation runs over all possible subsets  $S$  of features, excluding feature  $i$ . The function  $f(S)$  is defined as:

$$f(S) = \int f(x_1, \dots, x_p) dP_{x_{\notin S}} - E(f(X))$$

where  $f(x_1, \dots, x_p)$  is the model's prediction over all features in  $S$ ,  $dP_{x_{\notin S}}$  is the marginal distribution over the features not present in  $S$  (missing features). The integral term accounts for the expected model output by averaging over all possible values of the missing features, based on their marginal distribution.  $E(f(X))$ , represents the expected value of the model's output on the full feature vector, which serves as the baseline reference. The sum of all Shapley values  $\phi_i$  is equal to the difference between the model's output and the expected output at the baseline  $E(f(X))$ . Each individual value represents the contribution of the specific feature to this difference.

## Implementation

### Data processing

The datasets used for training were preprocessed to ensure they were appropriately formatted for input into an AE model. The first step involves collecting the data from the monitoring software of the digital twin system (Figure 3), either in real time while the reactor is in operation, or at a later time by identifying reactor operation time periods. Each dataset was normalized using a Min-Max scaler to a range between 0 and 1. To ensure consistent scaling across all datasets, the minimum and maximum values for each feature were derived from the last 3 years of reactor operation. During training, each dataset, representing a distinct reactor operation, is converted on the fly into 3D tensors and fed to the AE model. The tensors are constructed by sliding a window one second at a time across the dataset, regardless of its length, as shown in Figure 10. This process generates tensors of dimensions (batch size x window length x features). This format is well-suited for training MTS data, as it ensures that during testing, the model consistently considers the past window of seconds at each time step and reconstructs the same window length for further analysis. The optimal window length was found to be 10 seconds.

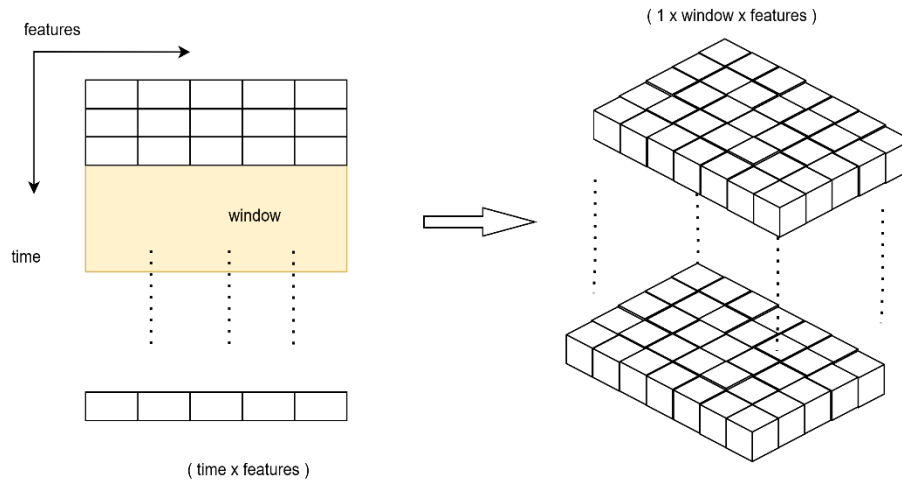


Figure 10: Tensors created for training by sliding a window forward one second at each step. This process creates (data length-window) tensors with dimensions (1 x window size x features).

### Training, tuning, implementation

We initially trained the AE model on the full cycle data to allow it to learn the reactor dynamics, followed by transfer learning on the SCRAM dataset to refine the detection of changes under sudden and extreme signal variability. To optimize the AE architecture, hyperparameter tuning was performed using Bayesian optimization [69]. Hyperparameter tuning is considered a necessary step in any ML application, as the choice of hyperparameters highly affects the model's performance [70]. Bayesian optimization was chosen among other common methods (e.g., grid search, random search, etc.) due to the noisy nature of the data and the depth of the architecture employed.

The AE architecture is designed to be flexible in hyperparameter tuning. The choices include the depth and width of the LSTM layers across the encoder, the decoder, and the latent representation. The search space includes a range of values for the hidden layers, the possible units per layer, the batch size, the dropout regularization to reduce overfitting, and the learning rate. Table 2 shows the optimal set of hyperparameters found through tuning. Out of the 47 datasets of the full reactor cycle, 34 datasets were used for training during hyperparameter optimization, 10 were used for validation, and the remaining 3 were used for testing after hyperparameter tuning was completed. The tuner evaluated 20 different hyperparameter combinations from the predefined search space, with each model trained for 30 epochs. The criterion for the optimal selection was to minimize the Mean Squared Error (MSE) on the validation loss. The optimal architecture is presented in Table 2 and Figure 11. Figure 12 presents the training and validation loss during training for the optimal architecture.

Table 2: Hyperparameters for the Autoencoder model

Hyperparameter	
Learning Rate	0.000352
Encoder Hidden Layer #1	256 neurons
Dropout Layer	0.1
Encoder Hidden Layer #2	128 neurons
bottleneck	32 neurons
Decoder Hidden Layer #1	128 neurons
Dropout Layer	0.2
Decoder Hidden Layer #2	128 neurons
Batch size	32
Window size	10

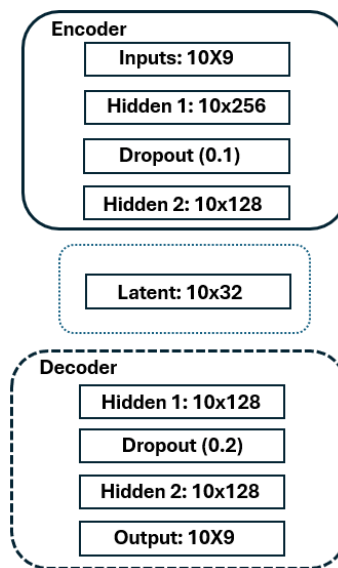


Figure 11: Structure diagram for the AE architecture.

A Python package, called Nuclear-replay-attack-detection, accompanies this paper and is publicly available at <https://github.com/Kvasili/Nuclear-replay-attack-detection>. It includes an example of running the proposed framework on the data used to simulate replayed attacks. The training, testing, and tuning make use of the Tensorflow, Keras, scikit-learn, and Pandas libraries. Simulations were run on an NVIDIA GeForce GTX 1650 Ti, with a training time of approximately 4 hours for 30 epochs on the full cycle datasets.

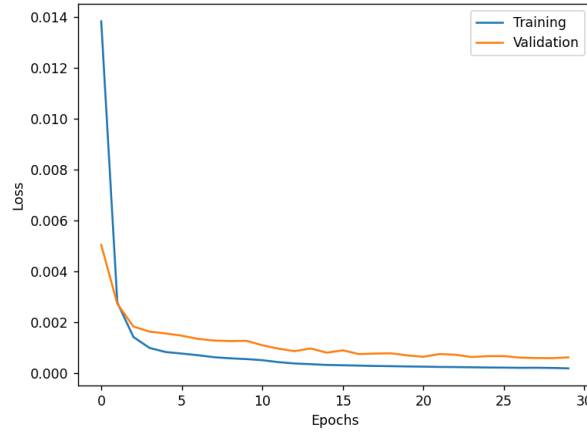


Figure 12: Training validation loss for the optimized architecture on the full cycle dataset.

To gain an understanding of the model’s performance on new unseen data, the trained network was applied to the 3 testing datasets. Figure 13 shows a comparison between the reconstructed and original data for the neutron counts (ch.1 feature) of the testing dataset. The model is able to reconstruct the signal adequately, proving that the reconstructive modeling of reactor behavior is successfully addressed. During steady state, the model consistently returns very low errors, while spikes are observed when reactor conditions change, particularly during startup and shutdown, when extreme transients occur. This means that during these events, a disagreement between the model and the actual behavior may lead to high reconstruction errors, which, in turn, will allow the identification of potential anomalies.

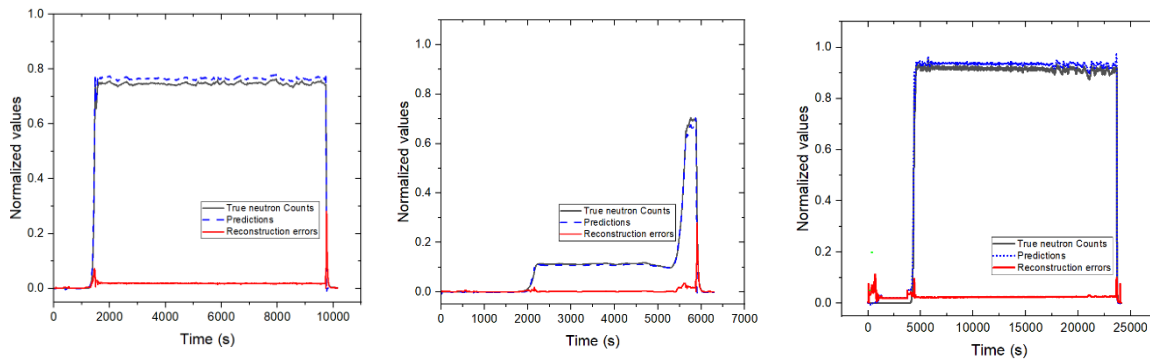


Figure 13: Reactor reconstructive modeling on the testing dataset.

### Fine-tuning on the SCRAM dataset

Training the models with the full cycle datasets showed that this is not adequate to fully adjust to the reactor dynamics during the extreme signal variability of a SCRAM process. Furthermore, the limited number of SCRAM events alone is estimated to affect the performance of the models to detect attacks under this process. To address this problem, the optimized network was further tuned on the SCRAM dataset, following the same network architecture and hyperparameters defined during tuning, and the same logic for preprocessing the data. As described, the dataset consists of 24 events of roughly 800 seconds each, with the SCRAM duration reflected in the signals between

300 and 400 seconds (Figure 7). This process fine tunes the network’s weights and biases to the dynamics of the SCRAM process, enhancing its ability to detect any deviations from expected patterns when exposed to falsified or erroneous data. Out of the 24 datasets, 20 were used for the training and 4 for the validation. The steps described in the last two sections represent the reconstructive modeling of reactor behavior of our methodology.

### Reconstruction error analysis

This step serves as the implementation of the second module in our methodology. The model’s loss objective is to minimize the reconstruction errors of sequences representing normal operation during training, in order to accurately reconstruct normal features and inaccurately reconstruct erroneous features during testing. Anomalies can be detected by evaluating the magnitude of either the MSE or the MAE, given by the following formulas, respectively:

$$MSE = \frac{1}{N} \sum (X - X')^2$$

$$MAE = \frac{1}{N} \sum |X - X'|$$

Where N is the number of samples in the training set, representing the number of tensors created. X is the vector containing the sensor values at a specific window and X' is the vector with the predicted values. Following the logic applied in relevant studies [60] [62], the threshold for defining an anomaly is determined by the distribution of MSE or MAE on the normal data. Observing the distribution, one can assess how well the model reconstructs the sequences and define a threshold above which a sequence is identified as a non-normal pattern. Figures 14.a and 14.b show the reconstruction error distribution by calculating the MAE on the data sequences for the training and the validation datasets. To investigate the performance, we also provide the error distribution in one of the falsified datasets that simulate the replay attack. The visualization reveals almost identical, skewed to the left, normal distributions for both the training and validation datasets, with the vast majority of the reconstructed sequences located close to the zero bin. This indicates the network’s success in reconstructing and predicting accurate values. Error values are also observed in the range larger than 0.2, but with a much smaller frequency of appearance. These values can be attributed to the noise inherent in the system or other sensor artifacts. As a sample result, Figure 14c presents the error distribution on an unseen falsified dataset, as if the analysis were to be performed after the attack. The pattern differs significantly from the distribution in the normal datasets. Although there is a large concentration of errors in the small value bins, which falls into the statistical uncertainty of the normal datasets, a significant concentration of large errors is also observed around the 0.4 bin. This suggests that a portion of the sequences clearly deviates from the expected behavior and, therefore, a potential anomaly is present in the system.

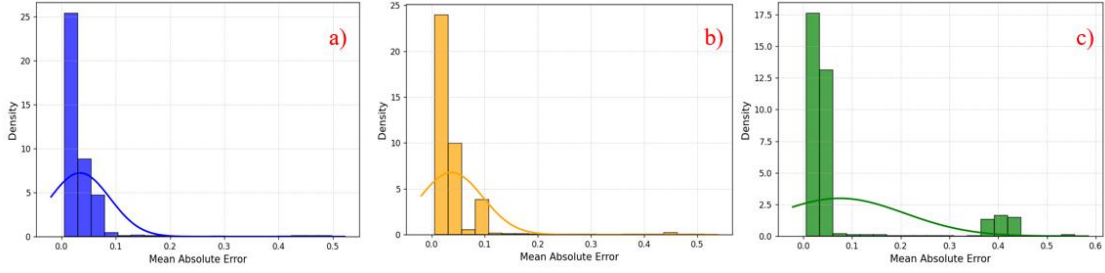


Figure 14: Reconstruction error distributions for training (a), validation (b), and testing (c) datasets.

### XAI implementation

SHAP analysis was initially introduced as a model-agnostic approach to provide general interpretability for any ML model prediction [67] [68]. Applying SHAP directly to MTS data leads to increased computational cost, especially as the number of features increases, as it would require the estimation of Shapley values over all combinations of feature-time datapoints. In addition, can mask overall trends by distributing contributions among too many timesteps. To overcome this shortcoming, a windowSHAP approach was proposed in this study [71], which restricts the calculation to distinct temporal windows. This approach reduces the complexity while preserving interpretability when explanations are required in a specific time sequence. The general formula is:

$$S_{window} = \bigcup_{i=1}^n \bigcup_{j=1}^m x_i(t - W_j : t - W_j + k)$$

Where  $\bigcup$  represents the union across all features and windows,  $x_i$  is the  $i$ -th feature in the MTS,  $W_j$  is the offset for the  $j$ -th window,  $k$  is the window size, and  $x_i(t - W_j : t - W_j + k)$  is a sequence of the feature  $x_i$ . In practice, this formula calculates Shapley values per window, identifying the timesteps and features within that window that have the most influence on the model's output.

For our case, windowSHAP needed to be modified to account for the specifics of the AE and the dynamics of the critical event in the reactor system. Instead of applying windowSHAP directly to the entire MTS, which raises concerns for real-time detection, we applied the modified version in real time to the reconstructed sequences flagged as anomalous (Figure 9). In addition, windowSHAP occludes data by replacing the "missing" values from a defined subwindow with the global average. This would not work well for our case because occluded values represent a baseline and expected behavior of the feature. In contrast, a SCRAM can be initiated at any time during reactor operation, often at a power level sufficiently far from the mean. A sudden change in power back to the global mean would not represent the expected baseline reactor behavior in this context. To accurately describe the baseline condition during a SCRAM event, it was set as the expected signal behavior for all signals in the dataset during the

event (Figure 15) and is dynamically updated over time to account for signal variability as the event evolves. In this way, the algorithm assigns importance to features whose evolution over the input time window causes the greatest change in error.

The interpretation of Shapley values is highly affected by the selection of the baseline data. Negative Shapley values indicate that a change in a certain feature decreases the error, suggesting a correlation with the predicted signal. Positive Shapley values indicate that a change in an input feature increases the error, suggesting a lack of correlation with the predicted signal. Shapley values near zero indicate that the signal is at the baseline or that the variation from the baseline did not influence the error [28]. By applying the modified WindowSHAP as long as the reconstruction error is triggered, a pattern emerges in the Shapley values of each feature during a replay attack, providing an indicator to distinguish this specific abnormality from other types, such as FDI or sensor malfunctions. This approach is less computationally expensive than the distance profile matrix methods used in relevant studies, where the current flagged sequence is compared with all possible sequences from past time steps.

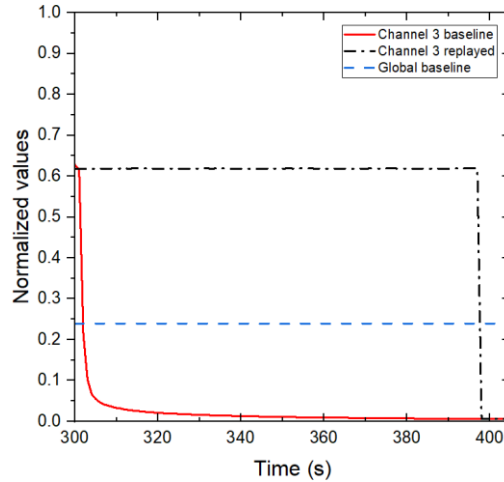


Figure 15: Comparison of replayed signal, expected behavior, and the global mean baseline for reactor power during the SCRAM event.

## Results

To detect anomalies effectively, we first need to determine the appropriate threshold that triggers detection of deviations from normal patterns. We analyze the error per second by evaluating the reconstruction error over a one-second sliding window with a width of 10 seconds. For each time step, the model computes the reconstruction error over the preceding 10-second window, and an anomaly is flagged if this error exceeds a defined threshold. Comparing the flagged anomaly with the true label, an anomaly detection metric is determined, showing the percentage of time steps in each dataset that exceed the error threshold. Table 3 shows the results for varying error thresholds between 0.05 and 0.25 for each of the datasets. The optimal error threshold would normally be determined by validating only the normal dataset, since in a real time scenario the abnormal data are not known. However, results are shown for both the normal and abnormal datasets to assess the AE's ability to capture anomalies. From

Table 3, for an error threshold between 0.1 and 0.2, the accuracy falls within the range 93-98% for the normal dataset. Setting the threshold at 0.15 yields a detection accuracy of more than 96% across all datasets.

Table 3: Detection Accuracy for Various Thresholds

Threshold	Normal	Replay#1	Replay#2	Replay#3	Replay#4	Replay#5	Replay#6
0.05	0.65	0.77	0.77	0.77	0.77	0.77	0.77
0.1	0.93	0.97	0.97	0.97	0.97	0.97	0.97
0.11	0.94	0.97	0.97	0.97	0.97	0.97	0.97
0.12	0.95	0.96	0.97	0.97	0.97	0.97	0.97
0.13	0.95	0.96	0.97	0.97	0.97	0.97	0.97
0.14	0.96	0.96	0.97	0.97	0.97	0.97	0.97
0.15	0.97	0.96	0.97	0.97	0.97	0.98	0.98
0.2	0.98	0.88	0.97	0.98	0.97	0.98	0.98
0.25	0.98	0.86	0.91	0.98	0.98	0.98	0.98

Even though the AE architecture can effectively identify deviations from normal reactor behavior, this does not guarantee that an identified anomaly is a replay attack. Time windows that exceed the threshold are passed to the XAI module for further analysis.

The XAI module is using the modified windowSHAP algorithm to evaluate the contribution of each feature at each time step on the reconstruction error of the flagged window. More specifically, each Shapley value represents a signal's contribution to the difference between the reconstruction error of the flagged window and the reconstruction error obtained when its baseline behavior is substituted for that signal. A negative Shapley value for signal  $x$  at time  $t$  indicates that this portion of the signal is correlated with the expected signal behavior found in the baseline (Figure 15), since it tends to lower the error. A positive value indicates that the signal  $x$  at time  $t$  deviates from the baseline behavior, since it tends to increase the error. A value close to zero indicates an agreement with the baseline. After extracting the Shapley values in each flagged 10-second window, those are averaged to provide a single value per second per signal/feature.

A pattern emerges when analyzing the Shapley values in the replayed sequences. Figure 16 shows the Shapley values at time steps where the reconstruction error exceeds the threshold, which occurs correctly during the falsification of the signals (300-400 s) in all 6 cases. For the three signals measuring neutron counts (ch.1), reactor power (ch.3), and neutron flux (ch.4), the Shapley values start at zero and increase linearly over the first 15 seconds, which matches the time required for these signals to drop to small values. This indicates a linearly increasing disagreement between the expected behavior, which should be dropping rapidly, and the replayed behavior, which has repeated steady state patterns. For the next 80 seconds, Shapley values exhibit a constant, repeated pattern, indicating a stable level of disagreement between the repeated and the expected signals, which have now been stabilized to small values. Finally, once the attack ends at 100 seconds, the Shapley values drop rapidly to near

zero, indicating that the disagreement decreases until the signals return to their expected values. The pattern is similar in all cases, indicating the same type of attack, with an increasing number of signals affected in each case. In all cases, the expected values are drawn from the baseline signals.

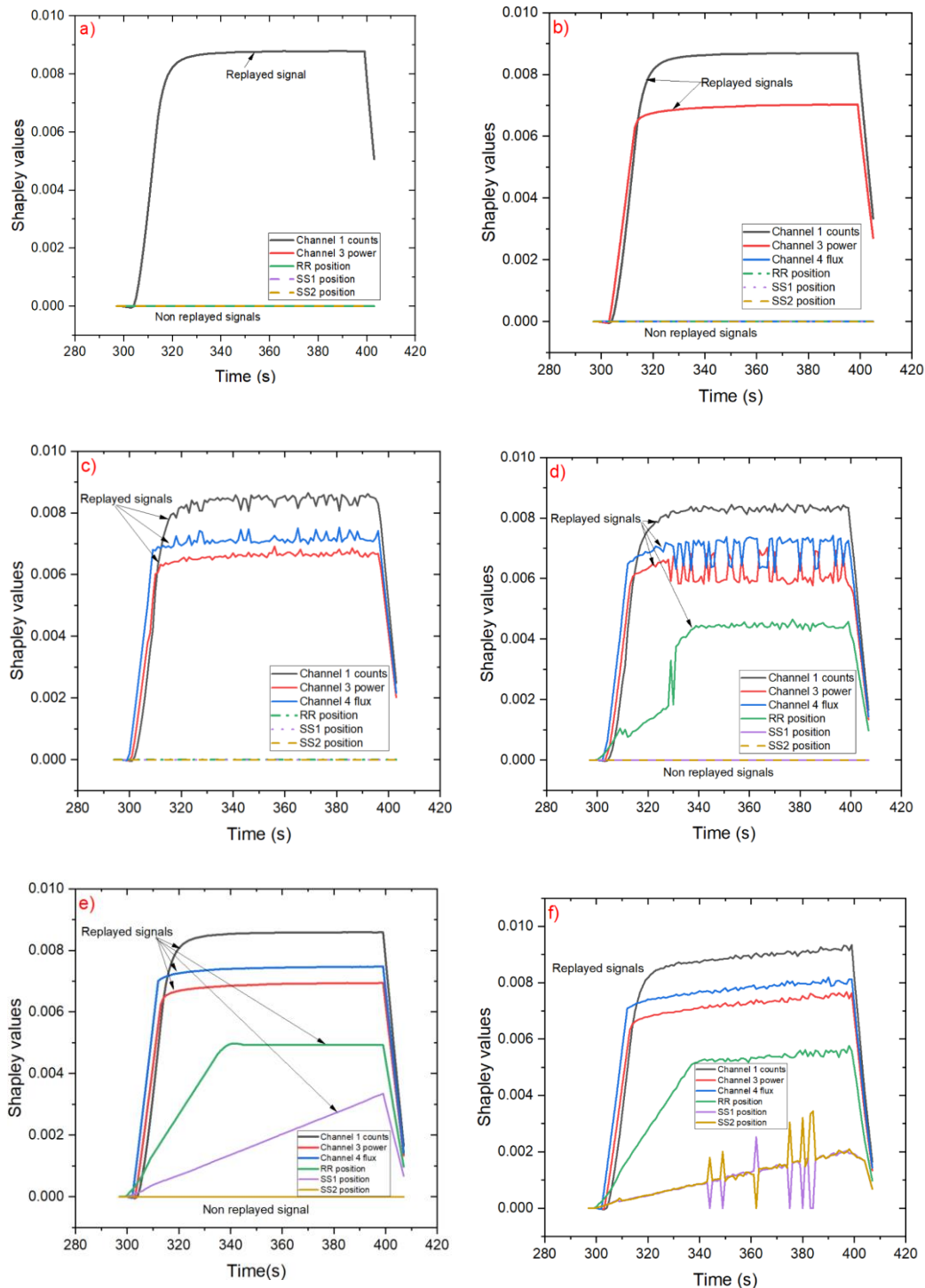


Figure 16: Shapley values per second per feature for the duration of the attack for a) Replay#1, b) Replay#2, c) Replay#3, d) Replay#4, e) Replay#5, f) Replay#6 cases.

For the three signals measuring the control rod positions, a similar pattern is observed. The rr rod (green line in Figure 16d-e-f) is rapidly inserted into the core during the SCRAM event, while the falsified signal remains steady for the entire duration. The Shapley values show a near linear disagreement for the first 30 seconds, matching the time required for the rr rod drivers to show the effect. Then, the Shapley values are steady, indicating a steady disagreement between the actual signal, which is now fully inserted, and the high values in the replayed signal. For the last few seconds, the Shapley values drop quickly and linearly as the signals return to their normal values at the end of the attack. For the SS1 and SS2 rods, the Shapley values (purple and yellow lines in Figure 16e-f) show a nearly linear increase in disagreement for almost the entire duration of the attack. This matches the behavior of the steady, replayed signals and the actual signals, which are dropping linearly until a few seconds before the end of the attack, when the Shapley values drop rapidly. Although the general trend is linear, some spikes are observed in the SS1 and SS2 Shapley values for the last case (Figure 16f), which can be attributed to outliers due to signal noise.

As observed, increasing the number of falsified signals results in smaller Shapley values for each additional signal at every time step. This can be attributed to the distribution of the reconstruction error difference across a larger number of signals in each case, where the most influential signals contribute more significantly to the overall deviation between the falsified signals and the baseline. Lastly, the repeated patterns observed in the extracted Shapley values across all falsified signals directly result from the repetitive nature of the replay attack. In the case of a different falsification (e.g. an FDI attack), the Shapley values are expected to exhibit different patterns and interpretations. This distinction supports the conclusion that the detected intrusion corresponds to a replay attack. A promising research direction would be to investigate how the distribution of Shapley values across time and feature space changes as the type of falsification changes.

Figures 17-22 present the visualization of the above logic. The signals are normalized and presented to the framework in real time, and for the last 10 seconds the reconstruction error is calculated from the first and second module. If the error falls below the threshold, the window is colored green, otherwise it is colored red. In case an abnormality is flagged, the XAI module is activated to analyze the patterns in the 10 second window and identify any falsified signals, highlighting them in red. After the attack ends, the framework reveals the timing, duration, and number of signals that have been replayed. Table 4 shows that over 95% of each replayed signal's length is correctly identified across all cases, with only minor misclassifications occurring at the beginning and end of the attack. Frame (f) in each figure shows the final set of detected replayed signals, correctly ranging from one to six. In frame (c) it is shown that, although the module flags an anomaly, the SHAP analysis does not indicate any disagreement with the expected signal behavior. This occurs at the start of the SCRAM process, when signal variability has not yet emerged and a clear pattern (normal or abnormal) has not been established. After the first 10 seconds, when the patterns begin to emerge, the XAI module consistently identifies the replayed signals across all cases. Also, in frame (f)

the falsified signals appear to extend for approximately 10 seconds after the attack, across all cases. This can be attributed to the framework's use of a 10 second window, in which the average Shapley value across the window is used to characterize each second. As a result, even if only one high value exists while the others are zero, the window may still be flagged as abnormal and replayed. The effect quickly vanishes when the entire window contains no high Shapley values, as seen immediately after the attack ends in frame (f).

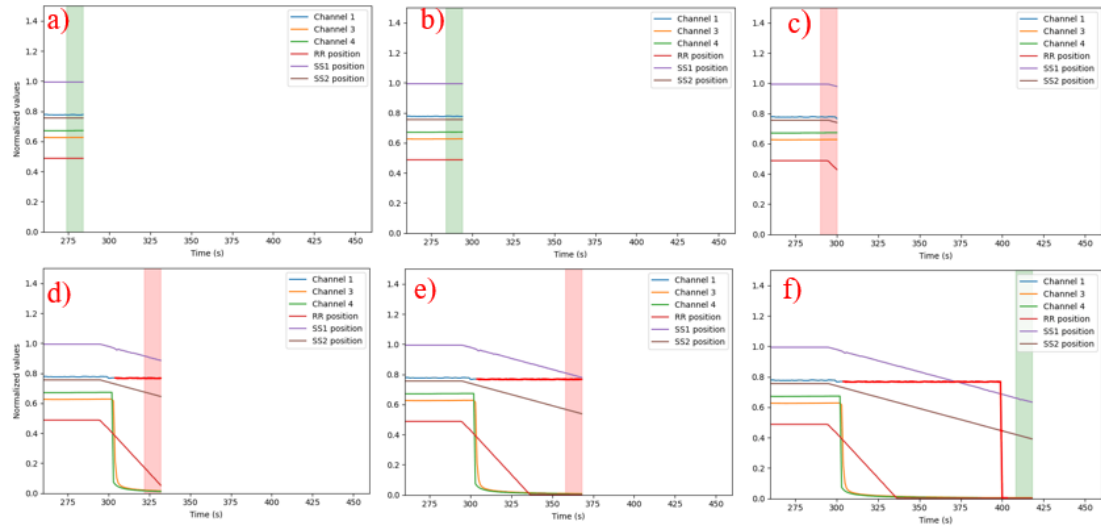


Figure 17: Replay attack detection for Replay#1 dataset.

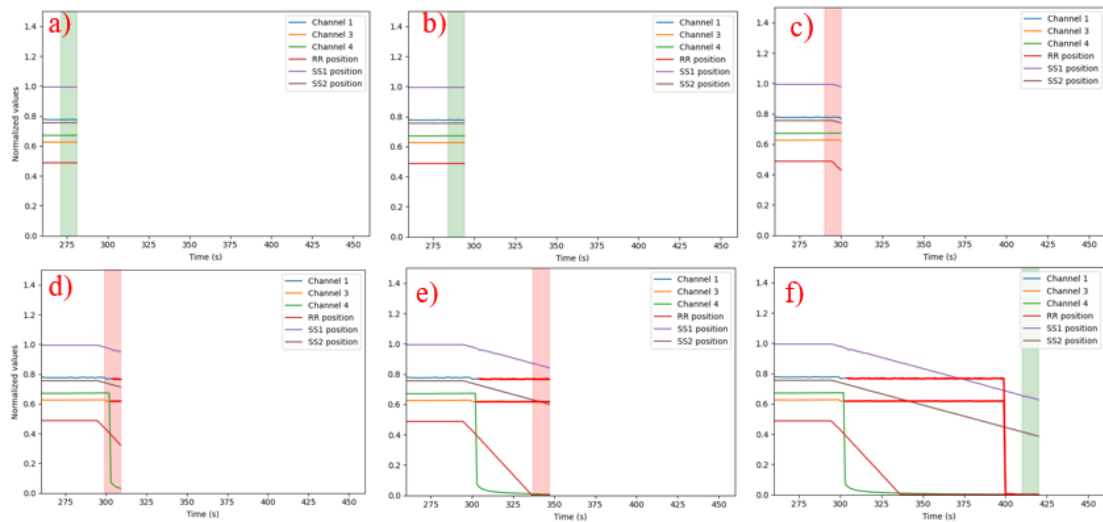


Figure 18: Replay attack detection for Replay#2 dataset.

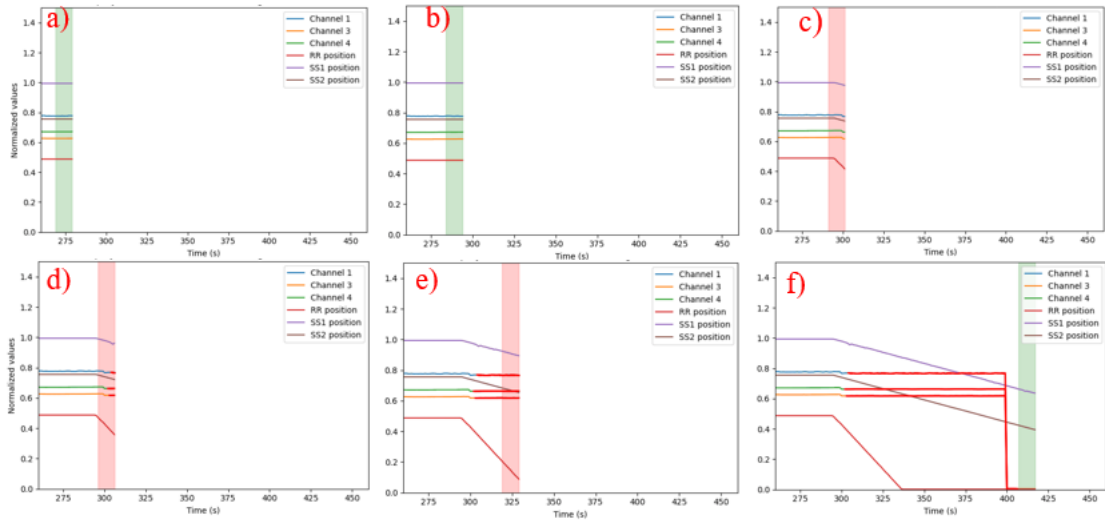


Figure 19: Replay attack detection for Replay#3 dataset.

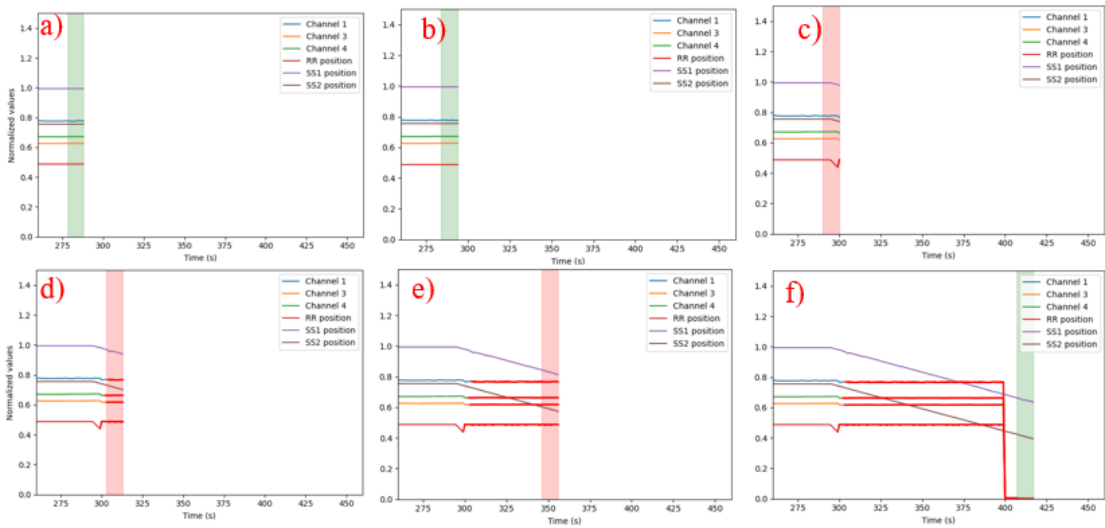


Figure 20: Replay attack detection for Replay#4 dataset.

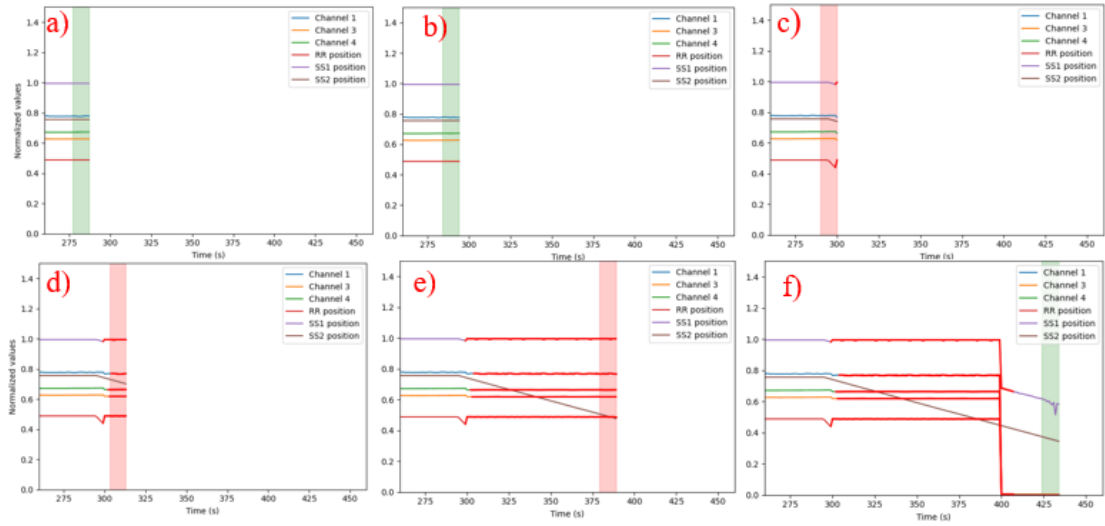


Figure 21: Replay attack detection for Replay#5 dataset.

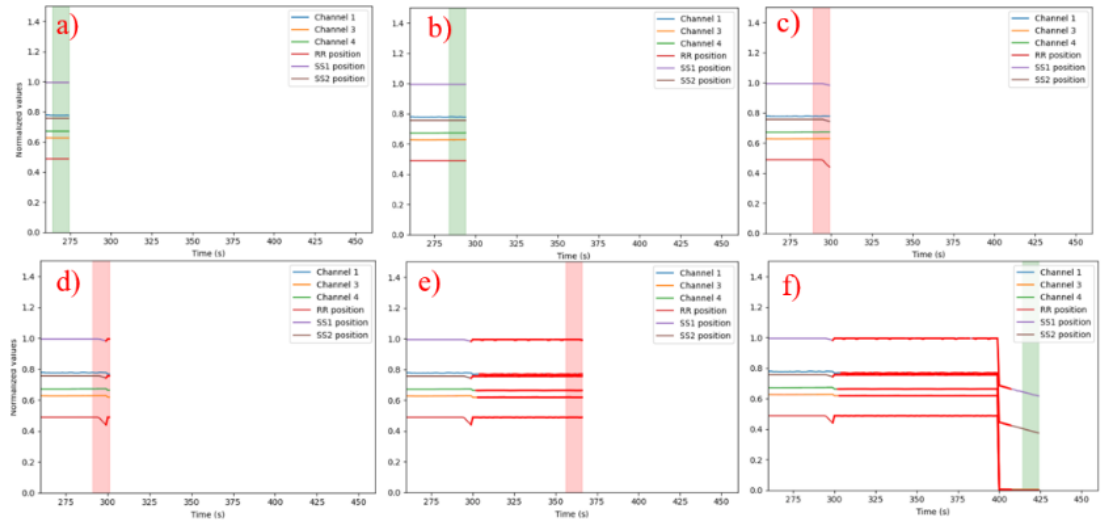


Figure 22: Replay attack detection for Replay#6 dataset.

Table 4: Percentage of each signal accurately identified as replayed per dataset

	Accuracy					
	Replay#1	Replay#2	Replay#3	Replay#4	Replay#5	Replay#6
Channel 1	95%	95%	95%	95%	95%	95%
Channel 3		96%	96%	96%	96%	96%
Channel 4			97%	97%	97%	97%
RR				99%	99%	99%
SS1					99%	99%
SS2						99%

## Conclusions

In this work, we propose a replay attack detection and localization framework that integrates an optimized deep AE architecture for nuclear MTS data, with a modified XAI module based on a windowSHAP algorithm. The network is trained solely on normal reactor data, eliminating the need to manually label and define training classes. We focus on a dynamic and time evolving use case of reactor operation to simulate the attack, with an increasing number of falsified signals ranging from one up to six concurrent signals. The results show success in triggering the abnormality, identifying the number of replayed signals, and the duration of the falsification in each signal within a single unified framework.

Although the framework was benchmarked on real-world datasets from PUR-1, it is estimated that it can be applicable to a wide range of practical scenarios where the expected signal behavior is known and can be used as a reference. Potential applications may include sensor drift detection, trajectory correction, and anomaly detection in multisensory environments. It is not our intention to distinguish in depth between a replay attack and other abnormalities that seemingly may have the same effect e.g. a sensor malfunction or FDI, because the problem has adequately been addressed in relevant studies by using rule-based [28] or matrix-based profile methods [26] for a single sensor. Instead, we present an effective and robust approach to a sophisticated multisensory anomaly detection scenario under a time evolving reactor operation, where the expected dynamics are known, all within a single framework. Moving forward, we acknowledge that post hoc explanations can have caveats in terms of computational cost. As future work, we aim to investigate the extent to which the number of falsified signals affects the performance in real time settings, and we intend to assess the framework's generalizability to other anomaly detection tasks.

## Acknowledgements

This research was performed using funding received from the DOE Office of Nuclear Energy's Nuclear Energy University Program under contract DE-NE0009268.

## References

- [1] L. Lin *et al.*, "Development and assessment of a nearly autonomous management and control system for advanced reactors," *Ann. Nucl. Energy*, vol. 150, p. 107861, Jan. 2021, doi: 10.1016/j.anucene.2020.107861.
- [2] R. T. Wood, B. R. Upadhyaya, and D. C. Floyd, "An autonomous control framework for advanced reactors," *Nucl. Eng. Technol.*, vol. 49, no. 5, pp. 896–904, Aug. 2017, doi: 10.1016/j.net.2017.07.001.
- [3] S. M. Cetiner *et al.*, "Supervisory Control System for Multi-Modular Advanced Reactors," Oak Ridge National Laboratory (ORNL), Oak Ridge, TN (United States), ORNL/TM-2016/693, Nov. 2016. doi: 10.2172/1615832.

- [4] K. Gkouliaras, V. Theos, Z. Dahm, W. Richards, K. Vasili, and S. Chatzidakis, "False Data Injection Detection in Nuclear Systems Using Dynamic Noise Analysis," *IEEE Access*, vol. 12, pp. 94936–94949, 2024, doi: 10.1109/ACCESS.2024.3425270.
- [5] R. Appiah *et al.*, "Development of a Cloud-based Application to Enable a Scalable Risk-informed Predictive Maintenance Strategy at Nuclear Power Plants," Idaho National Laboratory (INL), Idaho Falls, ID (United States), INL/RPT-22-70543-Rev000, Dec. 2022. doi: 10.2172/1906501.
- [6] A. Teixeira, D. Pérez, H. Sandberg, and K. H. Johansson, "Attack models and scenarios for networked control systems," in *Proceedings of the 1st international conference on High Confidence Networked Systems*, in HiCoNS '12. New York, NY, USA: Association for Computing Machinery, Apr. 2012, pp. 55–64. doi: 10.1145/2185505.2185515.
- [7] "Industrial Control Systems: Cyberattack trends and countermeasures - ScienceDirect." Accessed: May 22, 2025. [Online]. Available: [https://www.sciencedirect.com/science/article/pii/S0140366419319991?casa\\_token=twkMU9ykgwIAAAAA:sH8FKeMQ-lkkDkhf5popVKkrTpTYII33MXoW25jTaKzLkiGZlsf-4uhwgC4e-3wEWXr-c8EVFwM](https://www.sciencedirect.com/science/article/pii/S0140366419319991?casa_token=twkMU9ykgwIAAAAA:sH8FKeMQ-lkkDkhf5popVKkrTpTYII33MXoW25jTaKzLkiGZlsf-4uhwgC4e-3wEWXr-c8EVFwM)
- [8] H. S. Cho and T. H. Woo, "Cyber security in nuclear industry – Analytic study from the terror incident in nuclear power plants (NPPs)," *Ann. Nucl. Energy*, vol. 99, pp. 47–53, Jan. 2017, doi: 10.1016/j.anucene.2016.09.024.
- [9] A. Ayodeji, M. Mohamed, L. Li, A. Di Buono, I. Pierce, and H. Ahmed, "Cyber security in the nuclear industry: A closer look at digital control systems, networks and human factors," *Prog. Nucl. Energy*, vol. 161, p. 104738, Jul. 2023, doi: 10.1016/j.pnucene.2023.104738.
- [10] M. Baezner and P. Robin, "Stuxnet," ETH Zurich, Oct. 2017. doi: 10.3929/ETHZ-B-000200661.
- [11] J. P. Farwell and R. Rohozinski, "Stuxnet and the Future of Cyber War," *Survival*, Feb. 2011, Accessed: May 22, 2025. [Online]. Available: <https://www.tandfonline.com/doi/abs/10.1080/00396338.2011.555586>
- [12] D. Livingstone, C. Baylon, and R. Brunt, "Cyber Security Risks at Civil Nuclear Facilities," Oct. 2015, Accessed: Aug. 11, 2025. [Online]. Available: <https://policycommons.net/artifacts/1423397/cyber-security-at-civil-nuclear-facilities/2037664/>
- [13] B. Kesler, "The Vulnerability of Nuclear Facilities to Cyber Attack; Strategic Insights: Spring 2010," vol. 10, no. 1, 2011.
- [14] "A Robust Cybersecurity Solution Platform Architecture for Digital Instrumentation and Control Systems in Nuclear Power Facilities." Accessed: Aug. 11, 2025. [Online]. Available: <https://www.tandfonline.com/doi/epdf/10.1080/00295450.2019.1666599?needAccess=true>
- [15] P. N. Sema, P. Zavorsky, and R. Ruhl, "A critical review of attack scenarios on the IAEA Technical Guidance NSS 17 Computer Security at Nuclear Facilities," in *World Congress on Internet Security (WorldCIS-2014)*, Dec. 2014, pp. 87–90. doi: 10.1109/WorldCIS.2014.7028173.
- [16] "Research Challenges for the Security of Control Systems." Accessed: May 16, 2025. [Online]. Available: [https://www.usenix.org/legacy/event/hotsec08/tech/full\\_papers/cardenas/cardenas\\_html/](https://www.usenix.org/legacy/event/hotsec08/tech/full_papers/cardenas/cardenas_html/)
- [17] S. Amin, A. A. Cárdenas, and S. S. Sastry, "Safe and Secure Networked Control Systems under Denial-of-Service Attacks," in *Hybrid Systems: Computation and*

- Control*, R. Majumdar and P. Tabuada, Eds., Berlin, Heidelberg: Springer, 2009, pp. 31–45. doi: 10.1007/978-3-642-00602-9\_3.
- [18] O. Kosut, L. Jia, R. J. Thomas, and L. Tong, “Malicious Data Attacks on Smart Grid State Estimation: Attack Strategies and Countermeasures,” in *2010 First IEEE International Conference on Smart Grid Communications*, Oct. 2010, pp. 220–225. doi: 10.1109/SMARTGRID.2010.5622045.
- [19] Y. Liu, P. Ning, and M. K. Reiter, “False data injection attacks against state estimation in electric power grids,” *ACM Trans Inf Syst Secur*, vol. 14, no. 1, p. 13:1-13:33, Jun. 2011, doi: 10.1145/1952982.1952995.
- [20] Y. Mo and B. Sinopoli, “Secure control against replay attacks,” in *2009 47th Annual Allerton Conference on Communication, Control, and Computing (Allerton)*, Sep. 2009, pp. 911–918. doi: 10.1109/ALLERTON.2009.5394956.
- [21] Y. Zhao and C. Smidts, “A control-theoretic approach to detecting and distinguishing replay attacks from other anomalies in nuclear power plants,” *Prog. Nucl. Energy*, vol. 123, p. 103315, May 2020, doi: 10.1016/j.pnucene.2020.103315.
- [22] G. Liang, J. Zhao, F. Luo, S. R. Weller, and Z. Y. Dong, “A Review of False Data Injection Attacks Against Modern Power Systems,” *IEEE Trans. Smart Grid*, vol. 8, no. 4, pp. 1630–1638, Jul. 2017, doi: 10.1109/TSG.2015.2495133.
- [23] “An Event-Triggered Watermarking Strategy for Detection of Replay Attacks,” *IFAC-Pap.*, vol. 55, no. 6, pp. 317–322, Jan. 2022, doi: 10.1016/j.ifacol.2022.07.148.
- [24] J. Li, Z. Wang, Y. Shen, and L. Xie, “Attack Detection for Cyber-Physical Systems: A Zonotopic Approach,” *IEEE Trans. Autom. Control*, vol. 68, no. 11, pp. 6828–6835, Nov. 2023, doi: 10.1109/TAC.2023.3240383.
- [25] A. A. Elsaedy, N. Jagannath, A. G. Sanchis, A. Jamalipour, and K. S. Munasinghe, “Replay Attack Detection in Smart Cities Using Deep Learning,” *IEEE Access*, vol. 8, pp. 137825–137837, 2020, doi: 10.1109/ACCESS.2020.3012411.
- [26] S. Gargoum, N. Yassaie, A. W. Al-Dabbagh, and C. Feng, “A Data-Driven Framework for Verified Detection of Replay Attacks on Industrial Control Systems,” *IEEE Trans. Autom. Sci. Eng.*, vol. 22, pp. 3400–3415, 2025, doi: 10.1109/TASE.2024.3394315.
- [27] W. Wang, Y. Xie, L. Ren, X. Zhu, R. Chang, and Q. Yin, “Detection of data injection attack in industrial control system using long short term memory recurrent neural network,” in *2018 13th IEEE Conference on Industrial Electronics and Applications (ICIEA)*, May 2018, pp. 2710–2715. doi: 10.1109/ICIEA.2018.8398169.
- [28] Z. Dahm, V. Theos, K. Vasili, W. Richards, K. Gkouliaras, and S. Chatzidakis, “A one-class explainable AI framework for identification of non-stationary concurrent false data injections in nuclear reactor signals,” *Nucl. Eng. Des.*, vol. 444, p. 114359, Dec. 2025, doi: 10.1016/j.nucengdes.2025.114359.
- [29] I. Kiss, B. Genge, and P. Haller, “A clustering-based approach to detect cyber attacks in process control systems,” in *2015 IEEE 13th International Conference on Industrial Informatics (INDIN)*, Jul. 2015, pp. 142–148. doi: 10.1109/INDIN.2015.7281725.
- [30] R. Kumar, R. R. Hossain, S. Talukder, A. Jena, and A. T. A. Ghazo, “Recursive Histogram Tracking-Based Rapid Online Anomaly Detection in Cyber-Physical Systems,” *IEEE Trans. Syst. Man Cybern. Syst.*, vol. 52, no. 11, pp. 7123–7133, Nov. 2022, doi: 10.1109/TSMC.2022.3150304.
- [31] M. Ma, P. Zhou, D. Du, C. Peng, M. Fei, and H. M. AlBuflasa, “Detecting Replay Attacks in Power Systems: A Data-Driven Approach,” in *Advanced Computational Methods in Energy, Power, Electric Vehicles, and Their Integration*, K. Li, Y. Xue, S. Cui, Q. Niu, Z. Yang, and P. Luk, Eds., Singapore: Springer, 2017, pp. 450–457. doi: 10.1007/978-981-10-6364-0\_45.

- [32] Z. Zamanzadeh Darban, G. I. Webb, S. Pan, C. Aggarwal, and M. Salehi, "Deep Learning for Time Series Anomaly Detection: A Survey," *ACM Comput. Surv.*, vol. 57, no. 1, pp. 1–42, Jan. 2025, doi: 10.1145/3691338.
- [33] L. Antwarg, R. M. Miller, B. Shapira, and L. Rokach, "Explaining anomalies detected by autoencoders using Shapley Additive Explanations," *Expert Syst. Appl.*, vol. 186, p. 115736, Dec. 2021, doi: 10.1016/j.eswa.2021.115736.
- [34] J. H. Park, H. S. Jo, S. H. Lee, S. W. Oh, and M. G. Na, "A reliable intelligent diagnostic assistant for nuclear power plants using explainable artificial intelligence of GRU-AE, LightGBM and SHAP," *Nucl. Eng. Technol.*, vol. 54, no. 4, pp. 1271–1287, Apr. 2022, doi: 10.1016/j.net.2021.10.024.
- [35] K. Roshan and A. Zafar, "Utilizing XAI technique to improve autoencoder based model for computer network anomaly detection with shapley additive explanation(SHAP)," *Int. J. Comput. Netw. Commun.*, vol. 13, no. 6, pp. 109–128, Sep. 2021, doi: 10.5121/ijcnc.2021.13607.
- [36] "A Distributed Cyber-Attack Detection Scheme With Application to DC Microgrids." Accessed: Jun. 10, 2025. [Online]. Available: <https://ieeexplore.ieee.org/abstract/document/9054955>
- [37] "Novel fault diagnosis scheme utilizing deep learning networks," *Prog. Nucl. Energy*, vol. 118, p. 103066, Jan. 2020, doi: 10.1016/j.pnucene.2019.103066.
- [38] J. Yang and J. Kim, "An accident diagnosis algorithm using long short-term memory," *Nucl. Eng. Technol.*, vol. 50, no. 4, Art. no. 4, May 2018, doi: 10.1016/j.net.2018.03.010.
- [39] M. C. dos Santos *et al.*, "Deep rectifier neural network applied to the accident identification problem in a PWR nuclear power plant," *Ann. Nucl. Energy*, vol. 133, pp. 400–408, Nov. 2019, doi: 10.1016/j.anucene.2019.05.039.
- [40] H. A. Saeed, H. Wang, M. Peng, A. Hussain, and A. Nawaz, "Online fault monitoring based on deep neural network & sliding window technique," *Prog. Nucl. Energy*, vol. 121, p. 103236, Mar. 2020, doi: 10.1016/j.pnucene.2019.103236.
- [41] J. Park, T. Kim, and S. Seong, "Providing support to operators for monitoring safety functions using reinforcement learning," *Prog. Nucl. Energy*, vol. 118, p. 103123, Jan. 2020, doi: 10.1016/j.pnucene.2019.103123.
- [42] "Reactor," Nuclear Engineering - Purdue University. Accessed: Jun. 04, 2025. [Online]. Available: <https://engineering.purdue.edu/NE/research/facilities/reactor>
- [43] S. Chatzidakis *et al.*, "Characterizing Nuclear Cybersecurity States Using Artificial Intelligence/Machine Learning - Final Report".
- [44] V. Theos, K. Gkouliaras, and S. Chatzidakis, "Development and Analysis of a Real-time Digital Twin System in PUR-1," *Proc. Nucl. Plant Instrum. Control Hum.-Mach. Interface Technol. NPIC/MIT 2025 Chic. IL June 15-18 2025*, pp. 464–473, Jun. 2025, doi: doi.org/10.13182/NPIC/MIT25-46907.
- [45] R. B. Magadum, S. Bilagi, S. Bhandarkar, A. Patil, and A. Joshi, "Short-Term Wind Power Forecast Using Time Series Analysis: Auto-regressive Moving-average Model (ARMA)," in *Recent Developments in Electrical and Electronics Engineering*, P. Singhal, S. Kalra, B. Singh, and R. C. Bansal, Eds., Singapore: Springer Nature, 2023, pp. 319–341. doi: 10.1007/978-981-19-7993-4\_26.
- [46] Q. Yu, L. Jibin, and L. Jiang, "An Improved ARIMA-Based Traffic Anomaly Detection Algorithm for Wireless Sensor Networks," *Int. J. Distrib. Sens. Netw.*, vol. 12, no. 1, p. 9653230, Jan. 2016, doi: 10.1155/2016/9653230.
- [47] "CorrCorr: A feature selection method for multivariate correlation network anomaly detection techniques," *Comput. Secur.*, vol. 83, pp. 234–245, Jun. 2019, doi: 10.1016/j.cose.2019.02.008.

- [48] Z. Jadidi, S. Pal, M. Hussain, and K. Nguyen Thanh, "Correlation-Based Anomaly Detection in Industrial Control Systems," *Sensors*, vol. 23, no. 3, Art. no. 3, Jan. 2023, doi: 10.3390/s23031561.
- [49] A. Iliopoulos, J. Violos, C. Diou, and I. Varlamis, "Detection of Anomalies in Multivariate Time Series Using Ensemble Techniques," in *2023 IEEE Ninth International Conference on Big Data Computing Service and Applications (BigDataService)*, Jul. 2023, pp. 1–8. doi: 10.1109/BigDataService58306.2023.00007.
- [50] C. Zhang *et al.*, "A Deep Neural Network for Unsupervised Anomaly Detection and Diagnosis in Multivariate Time Series Data," *Proc. AAAI Conf. Artif. Intell.*, vol. 33, no. 01, pp. 1409–1416, Jul. 2019, doi: 10.1609/aaai.v33i01.33011409.
- [51] O. I. Provotar, Y. M. Linder, and M. M. Veres, "Unsupervised Anomaly Detection in Time Series Using LSTM-Based Autoencoders," in *2019 IEEE International Conference on Advanced Trends in Information Theory (ATIT)*, Dec. 2019, pp. 513–517. doi: 10.1109/ATIT49449.2019.9030505.
- [52] D. E. Rumelhart, G. E. Hinton, and R. J. Williams, "Learning representations by back-propagating errors," *Nature*, vol. 323, no. 6088, pp. 533–536, Oct. 1986, doi: 10.1038/323533a0.
- [53] M. Sakurada and T. Yairi, "Anomaly Detection Using Autoencoders with Nonlinear Dimensionality Reduction," in *Proceedings of the MLSDA 2014 2nd Workshop on Machine Learning for Sensory Data Analysis*, in MLSDA'14. New York, NY, USA: Association for Computing Machinery, Dec. 2014, pp. 4–11. doi: 10.1145/2689746.2689747.
- [54] Tayeh, Tareq, "An attention-based ConvLSTM autoencoder with dynamic thresholding for unsupervised anomaly detection in multivariate time series."
- [55] K. Pawar and V. Z. Attar, "Assessment of Autoencoder Architectures for Data Representation," in *Deep Learning: Concepts and Architectures*, W. Pedrycz and S.-M. Chen, Eds., Cham: Springer International Publishing, 2020, pp. 101–132. doi: 10.1007/978-3-030-31756-0\_4.
- [56] S. Hochreiter and J. Schmidhuber, "Long Short-Term Memory," *Neural Comput.*, vol. 9, no. 8, pp. 1735–1780, Nov. 1997, doi: 10.1162/neco.1997.9.8.1735.
- [57] N. M. Rezk, M. Purnaprajna, T. Nordström, and Z. Ul-Abdin, "Recurrent Neural Networks: An Embedded Computing Perspective," *IEEE Access*, vol. 8, pp. 57967–57996, 2020, doi: 10.1109/ACCESS.2020.2982416.
- [58] "The Vanishing Gradient Problem During Learning Recurrent Neural Nets and Problem Solutions." Accessed: Aug. 12, 2025. [Online]. Available: <https://www.worldscientific.com/doi/epdf/10.1142/S0218488598000094>
- [59] A. Sherstinsky, "Fundamentals of Recurrent Neural Network (RNN) and Long Short-Term Memory (LSTM) network," *Phys. Nonlinear Phenom.*, vol. 404, p. 132306, Mar. 2020, doi: 10.1016/j.physd.2019.132306.
- [60] "Unsupervised anomaly detection in pressurized water reactor digital twins using autoencoder neural networks," *Nucl. Eng. Des.*, vol. 413, p. 112502, Nov. 2023, doi: 10.1016/j.nucengdes.2023.112502.
- [61] "Development of deep autoencoder-based anomaly detection system for HANARO," *Nucl. Eng. Technol.*, vol. 55, no. 2, pp. 475–483, Feb. 2023, doi: 10.1016/j.net.2022.10.009.
- [62] P. Mena, R. A. Borrelli, and L. Kerby, "Detecting Anomalies in Simulated Nuclear Data Using Autoencoders," *Nucl. Technol.*, Jan. 2024, Accessed: Jun. 13, 2025. [Online]. Available: <https://www.tandfonline.com/doi/abs/10.1080/00295450.2023.2214257>

- [63] D. Hu, C. Zhang, T. Yang, and G. Chen, "Anomaly Detection of Power Plant Equipment Using Long Short-Term Memory Based Autoencoder Neural Network," *Sensors*, vol. 20, no. 21, Art. no. 21, Jan. 2020, doi: 10.3390/s20216164.
- [64] L. Lin, C. Walker, and V. Agarwal, "Explainable machine-learning tools for predictive maintenance of circulating water systems in nuclear power plants," *Nucl. Eng. Technol.*, vol. 57, no. 9, p. 103588, Sep. 2025, doi: 10.1016/j.net.2025.103588.
- [65] A. Barredo Arrieta *et al.*, "Explainable Artificial Intelligence (XAI): Concepts, taxonomies, opportunities and challenges toward responsible AI," *Inf. Fusion*, vol. 58, pp. 82–115, Jun. 2020, doi: 10.1016/j.inffus.2019.12.012.
- [66] O. Fink, Q. Wang, M. Svensén, P. Dersin, W.-J. Lee, and M. Ducoffe, "Potential, challenges and future directions for deep learning in prognostics and health management applications," *Eng. Appl. Artif. Intell.*, vol. 92, p. 103678, Jun. 2020, doi: 10.1016/j.engappai.2020.103678.
- [67] S. M. Lundberg and S.-I. Lee, "A Unified Approach to Interpreting Model Predictions," in *Advances in Neural Information Processing Systems*, Curran Associates, Inc., 2017. Accessed: Jun. 03, 2025. [Online]. Available: [https://proceedings.neurips.cc/paper\\_files/paper/2017/hash/8a20a8621978632d76c43dfd28b67767-Abstract.html](https://proceedings.neurips.cc/paper_files/paper/2017/hash/8a20a8621978632d76c43dfd28b67767-Abstract.html)
- [68] "Lundberg: Consistent individualized feature attribution... - Google Scholar." Accessed: Jun. 04, 2025. [Online]. Available: [https://scholar.google.com/scholar\\_lookup?title=Consistent%20Individualized%20Feature%20Attribution%20for%20Tree%20Ensembles&author=S.M.%20Lundberg&publication\\_year=2018](https://scholar.google.com/scholar_lookup?title=Consistent%20Individualized%20Feature%20Attribution%20for%20Tree%20Ensembles&author=S.M.%20Lundberg&publication_year=2018)
- [69] T. T. Joy, S. Rana, S. Gupta, and S. Venkatesh, "Hyperparameter tuning for big data using Bayesian optimisation," in *2016 23rd International Conference on Pattern Recognition (ICPR)*, Dec. 2016, pp. 2574–2579. doi: 10.1109/ICPR.2016.7900023.
- [70] L. Yang and A. Shami, "On hyperparameter optimization of machine learning algorithms: Theory and practice," *Neurocomputing*, vol. 415, pp. 295–316, Nov. 2020, doi: 10.1016/j.neucom.2020.07.061.
- [71] A. Nayebi, S. Tipirneni, C. K. Reddy, B. Foreman, and V. Subbian, "WindowSHAP: An Efficient Framework for Explaining Time-series Classifiers based on Shapley Values," May 08, 2023, *arXiv*: arXiv:2211.06507. doi: 10.48550/arXiv.2211.06507.